

2

# NAVAL POSTGRADUATE SCHOOL Monterey, California

AD-A275 704



**S** DTIC  
ELECTE  
FEB 18 1994  
**A**

## THESIS

THE VELOCITY FIELD  
IN THE NORTHEAST ATLANTIC  
FROM SATELLITE-TRACKED DRIFTING BUOYS

by

Paolo Giannetti

September 1993

Thesis Advisor:

Jeffrey D. Paduan

Approved for public release; distribution is unlimited.

94-05348



DTIC QUALITY INSPECTED 2

94 2 17 070

Unclassified

UNCLAS

## REPORT DOCUMENTATION PAGE

1a. REPORT SECURITY CLASSIFICATION Unclassified			1b. RESTRICTIVE MARKINGS N/A		
2a. SECURITY CLASSIFICATION AUTHORITY N/A			3. DISTRIBUTION AVAILABILITY OF REPORT Approved for public release; Distribution is unlimited.		
2b. DECLASSIFICATION/DOWNGRADING SCHEDULE					
4. PERFORMING ORGANIZATION REPORT NUMBER(S)			5. MONITORING ORGANIZATION REPORT NUMBER(S)		
6a. Name Of Performing Organization Naval Postgraduate School		6b. OFFICE SYMBOL 35	7a. NAME OF MONITORING ORGANIZATION Naval Postgraduate School		
6c. ADDRESS (city, state, and zip code) Monterey, CA 93943-5000			7b. ADDRESS (city, state, and zip code) Monterey, CA 93943-5000		
8a. NAME OF FUNDING/SPONSORING ORGANIZATION		8b. OFFICE SYMBOL (If Applicable)	9. PROCUREMENT INSTRUMENT IDENTIFICATION NUMBER		
8c. ADDRESS (city, state, and zip code)			10. SOURCE OF FUNDING NUMBERS		
			Program Element Number	Project No	Task No
			Work Unit Accession No		
11. TITLE (Include Security Classification) THE VELOCITY FIELD IN THE NORTHEAST ATLANTIC FROM SATELLITE-TRACKED DRIFTING BUOYS					
12. PERSONAL AUTHOR(S) Giannetti Paolo					
13a. TYPE OF REPORT Master's Thesis		13b. TIME COVERED From To		14. DATE OF REPORT (year, month, day) September 1993	
				15. PAGE COUNT 82	
16. SUPPLEMENTARY NOTATION The views expressed in this thesiss are those of the author and do not reflect the official policy or position of the Department of Defence or the U.S. Government.					
17. COSATI CODES			18. SUBJECT TERMS (continue on reverse if necessary and identify by block number)		
Field	Group	Subgroup	Drifting Buoys, Subduction, Lagrangian time scales, Lagrangian length scales, Diffusivity, Azores Current, Azores Front, ARGOS System, Eddy Kinetic Energy, Surface Currents		
19. ABSTRACT (continue on reverse if necessary and identify by block number)					
<p>Data from 36 surface drifters (Holey Socks) were collected for a period of 23 months from July 1991 to May 1993 in the Northeast Atlantic Ocean between the Azores Islands and the Canary Islands as a part of the SUBDUCTION experiment. The position information from those drifters is analyzed in this study to obtain horizontal velocity statistics at the drogue level (15m). Mean currents in the area are found to be less than 2 cm/sec except in the vicinity of the Azores Front where the 2-year mean eastward currents measure <math>3.9 \pm 1.7</math> cm/sec. Zonally-averaged northward currents are divergent over most of the area in contrast to the convergent surface currents expected in the region due to convergence of the climatological Ekman transport. It is shown, however, that array bias due to the non-uniform distribution of particles in the presence of an eddy field can account for this result. The mean eddy kinetic energy level is <math>103 \text{ cm}^2/\text{sec}^2</math> and the mean diffusivity is <math>5.0 \times 10^7 \text{ cm}^2/\text{sec}</math>. These values are in line with results from previous drifter studies. Mean Lagrangian integral time and length scales are 5.7 days and 48 km, respectively and, in all cases, east-west scales are greater than north-south scales. In general, this long data set is still dominated by the effects of mesoscale eddies. An objective method to select eddy portions of drifter trajectories is presented that may help to characterize the eddy field in future studies.</p>					
20. DISTRIBUTION/AVAILABILITY OF ABSTRACT			21. ABSTRACT SECURITY CLASSIFICATION		
<input checked="" type="checkbox"/> unclassified/unlimited <input type="checkbox"/> same as report <input type="checkbox"/> DTIC users			Unclassified		
22a. NAME OF RESPONSIBLE INDIVIDUAL Jeffrey D Paduan			22b. TELEPHONE (include area code) (408) 656-3350		22c. OFFICE SYMBOL OC/Pd

DD FORM 1473, 84 MAR

83 APR edition may be used until exhausted

SECURITY CLASSIFICATION OF THIS PAGE

All other editions are obsolete

Unclassified

Approved for public release; distribution is unlimited.

**The Velocity Field in the Northeast Atlantic from  
Satellite-Tracked Drifting Buoys**

by

**Paolo Giannetti**  
**Lieutenant Commander, Italian Navy**  
**B.S., Naval Academy, 1981**

Submitted in partial fulfillment of the  
requirements for the degree of

**MASTER OF SCIENCE IN PHYSICAL OCEANOGRAPHY**

from the

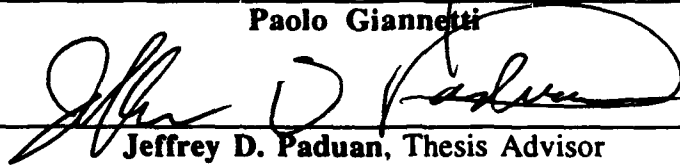
**NAVAL POSTGRADUATE SCHOOL**  
**September 1993**

Author:



**Paolo Giannetti**

Approved By:



**Jeffrey D. Paduan, Thesis Advisor**



**Curtis Collins, Second Reader**



**Curtis Collins, Chairman, Department of Oceanography**

## ABSTRACT

Data from 36 surface drifters (Holey Socks) were collected for a period of 23 months from July 1991 to May 1993 in the Northeast Atlantic Ocean between the Azores Islands and the Canary Islands as a part of the SUBDUCTION experiment. The position information from those drifters is analyzed in this study to obtain horizontal velocity statistics at the drogue level (15m). Mean currents in the area are found to be less than 2 cm/sec except in the vicinity of the Azores Front where the 2-year mean eastward currents measure  $3.9 \pm 1.7$  cm/sec. Zonally-averaged northward currents are divergent over most of the area in contrast to the convergent surface currents expected in the region due to convergence of the climatological Ekman transport. It is shown, however, that array bias due to the non-uniform distribution of particles in the presence of an eddy field can account for this result. The mean eddy kinetic energy level is  $103 \text{ cm}^2/\text{sec}^2$  and the mean diffusivity is  $5.0 \times 10^7 \text{ cm}^2/\text{sec}$ . These values are in line with results from previous drifter studies. Mean Lagrangian integral time and length scales are 5.7 days and 48 km, respectively and, in all cases, east-west scales are greater than north-south scales. In general, this long data set is still dominated by the effects of mesoscale eddies. An objective method to select eddy portions of drifter trajectories is presented that may help to characterize the eddy field in future studies.

Accession For	
NTIS OMA&I	✓
DTIC TAB	✓
Unannounced	✓
Justification	
By	
Distribution/	
Availability Code	
Dist	Avail and/or Special
A-1	

## TABLE OF CONTENTS

I. INTRODUCTION .....	1
II. DATA SET	
A. SATELLITE-TRACKED SURFACE DRIFTERS.....	6
B. LAGRANGIAN NATURE OF THE DRIFTERS .....	7
C. OVERVIEW OF THE DATA	
1. Spatial Coverage.....	8
2. Temporal Coverage .....	9
D. CONSIDERATION OF THE TRANSMITTER DUTY CYCLE.....	10
E. DESCRIPTION OF THE INTERPOLATION PROCEDURES .....	12
III. BASIC STATISTICS .....	25
A. LARGE AREA AND SEASONAL AVERAGES	
1. Mean Currents .....	26
2. Kinetic Energy.....	27
B. ZONAL AVERAGES.....	29
IV. SINGLE PARTICLE LAGRANGIAN STATISTICS .....	41
A. LAGRANGIAN AUTOCOVARIANCES .....	42
1. Integral Time Scales.....	44
2. Integral Length Scales .....	45
B. DIFFUSIVITY .....	46
1. Array Bias.....	49
C. POLARIZATION .....	51
V. EDDY SURVEY .....	61
A. SUBJECTIVE METHOD .....	61
B. OBJECTIVE METHOD .....	61
VI. CONCLUSIONS AND RECOMMENDATIONS	
A. CONCLUSIONS.....	67
B. RECOMMENDATIONS .....	69
REFERENCES .....	70
INITIAL DISTRIBUTION LIST.....	73

## **ACKNOWLEDGMENT**

I want to express my sincere gratitude to my thesis advisor Dr. Jeffrey D. Paduan for his huge support and personal involvement. He continuously inspired me during my first steps in the world of the "water followers". Many thanks are extended to the people who helped me during the preparation of this work. Particularly to my colleague and best friend Rogerio Chumbinho who patiently answered all my questions on programming. I would like to thank Mike Cook for helping me to prepare the figures, Pietro Stopponi for providing endless support and word processing help, and last but not least my coffee machine as the best company late at night.

Finally, I am most appreciative of my wife Laura and daughter Giulia to whom I dedicate this work for their support and for their recognition of the importance of my commitment to completing this thesis.

The data analyzed in this thesis was collected as part of the SUBDUCTION Experiment funded by the Office of Naval Research.



## I. INTRODUCTION

The upper ocean is often well-mixed in terms of its density and velocity properties. The depth of this "mixed layer" varies with season and location but is on the order of tens of meters thick. This depth layer is an important boundary layer where momentum and buoyancy are exchanged between the atmosphere and the deeper ocean below. Many oceanographic field programs have been conducted with the specific aim of describing the growth and decay of the mixed layer under various air-sea interactions (e.g. Tabata, 1965; Davis et al., 1981; Paduan and deSzoeki, 1986; Paduan et al, 1988). Even more studies have attempted to model the evolution of mixed layer depth, temperature, and velocity. The simplest of these models consider bulk mixed layers in which velocity and temperature are constant and parameterizations of turbulent kinetic energy at the mixed layer base are responsible for mixing (e.g. Kraus and Turner, 1967; Niiler and Kraus, 1977). Other models use Richardson number dependent mixing (e.g. Pollard et al. 1973; Price et al., 1986). In all cases, the one-dimensional assumptions limit the usefulness of the models over long time periods.

The development of low-orbit satellites with positioning sensors have made it possible to remotely-track the position of drifting buoys on the surface of the ocean. The time rate of change of drifter position gives estimates of the surface currents. Such measurements can be used to gain new information about the ocean mixed layer. Current measurements from drifting buoys are particularly well-suited to providing spatial information, although they usually do not provide measurements at more than one depth (Paduan and Niiler, 1993). Early deployments of satellite-tracked drifters provided basic information about surface currents and their variability in many regions (Kirwan et al., 1976; Kirwan et al., 1978; McNally, 1981; Krauss and Böning, 1987; Richardson, 1983).

More recently, it has been shown that the performance of drifting buoys as water followers depends critically on the design of the instrument. Niiler et al. (1987, 1993) describe actual measurements of slip past drogue elements for various drogue designs and



wind conditions. They show that both the shape of the drogue and its drag area relative to the drag area of the surface float plus tether are important parameters. The shape of the drogue must be rigid and symmetric so that the drogue does not produce an airfoil effect that could move it at an angle to the direction of the current. The drag of the drogue element must be large enough to overcome the drag of the surface float and tether, which can be strongly influenced by direct wind forcing. The drag characteristics of a drifter are characterized by the Drag Area Ratio,  $R$ , which gives the ratio of the drag of the drogue to the combined drag of the surface float plus tether. For properly constructed drifters with drag area ratios greater than 40, the current slip past the drogue (the error) is less than 2 cm/sec for wind speeds up to 20 m/sec. Early-generation drifters with low drag area ratios ( $R < 10$ ) had significant downwind slip, which led to some incorrect interpretations of the Ekman response in the mixed layer (McNally, 1981; McNally et al., 1989). Niiler and Paduan (1993) show that properly-constructed drifters approximate much more closely the theoretical motion in an Ekman boundary layer where water moves at right angles to the wind.

Luyten et al. (1983) presented a theoretical model for deep ocean circulation that has defined important links between that circulation and the processes in the mixed layer. These links occur in specific ocean areas where deep isopycnal surfaces are known to intersect the bottom of the mixed layer. This process is known as outcropping. The northeast Atlantic Ocean is an area where deep (subsurface) isopycnals extending from points south of the region outcrop at the surface. This observation is critical in light of the theory of Luyten et al. (1983). They have shown how south of the outcropping latitude, water motion within isopycnal layers can be predicted based on the conservation of potential vorticity, which is determined by layer thickness. This means that, given the distribution of deep isopycnal layers, deep ocean circulation can be simply modeled. Such deep information is difficult to obtain, however. A more practical starting point would be based on observations at the ocean surface, particularly in the forcing regions of outcropping isopycnals. If a predictive link could be made between mixed layer processes

in the outcrop region and the thickness of deep isopycnals, then deep circulation over much of the ocean depths could be predicted without deep measurements.

In order to understand the link between mixed layer processes and the distribution of deep isopycnals in an outcrop area, an oceanographic field program was sponsored by the Office of Naval Research (ONR) in the region of the Canary Basin in the northeast Atlantic. Many time series and survey measurements were made in the region, which extends from the Azores Islands in the north to the Canary Islands in the south and west to about 35° W. Measurements included moored current meters and meteorological sensors, deep isopycnal floats, ship-based CTD and SEASOAR surveys, tracer studies, and surface drifters. The measurements were concentrated in the two-year period from spring 1991 to 1993. The program was referred to as the SUBDUCTION Experiment. The name reflects the belief that, according to the theory of Luyten et al. (1983), water from the mixed layer must be finding its way into the upper thermocline in this area, setting the thickness properties of isopycnal layers. The process of downwelling water making its way into the thermocline is referred to as subduction. In this context, thermocline refers to the permanent thermocline below 100 m and not to the seasonal thermocline, which is expected to incorporate and release water from the mixed layer during the course of the seasonal cycle.

The Canary Basin is a likely area for subduction because, on average, the wind forcing produces Ekman convergence and downwelling velocities. The region of interest spans the latitude band where, climatologically, wind stress curl is negative as a result of westerlies in the northern portion of the area giving way to easterlies in the southern portion of the area. Therefore the surface wind-driven currents are expected to be convergent on average. Furthermore, most of the convergence is expected to result from north-south currents given the smaller east-west variability in the wind forcing. In such an area, zonal (east-west) averages of current should show a convergent pattern as a function of latitude.

This study concentrates on the trajectories of 36 satellite-tracked drifters that were deployed in the Canary Basin as part of the SUBDUCTION Experiment. The primary goal of the drifter measurements was to study the currents in the Ekman layer and, with the advantage of many thousands of observations over several years, attempt to observe the

expected surface convergence during a period when extensive meteorological and deeper hydrographic and float measurements were obtained. Drifters are a good way to attempt this difficult measurement because they have much shorter integral time scales than do moored instruments and they are relatively inexpensive. These factors mean that a large number of independent observations of surface velocity can be obtained from an array of drifting buoys. Large numbers of observations are required to measure mean currents and their divergence field in the mixed layer because of the large contributions by mesoscale eddies. (Mixed layer velocity variability is usually many times greater than mean currents.)

The process of subduction is not understood. One major question that exists is whether the process is a distributed one spread over the entire region or whether the process is concentrated at oceanographic fronts. A major oceanographic front, the Azores Front, is present in the SUBDUCTION region. The deployment and analysis of surface drifters was designed to look for convergent currents over large areas but also to look specifically at currents north and south of the historical location of the Azores Front, which has been observed between 32° N and 36° N in this area (Krauss and Käse, 1984; Gould, 1985; Stramma and Müller, 1989). Deployments were concentrated along latitude lines north and south of the frontal region in order to look for frontal convergence and possible asymmetry in the mean currents and eddy characteristics.

This thesis work presents the velocity statistics from the surface drifters deployed as part of the SUBDUCTION Experiment. The goals were to characterize the mean currents in the mixed layer of the SUBDUCTION region and, if possible, determine the convergence of the mean currents. It was also a goal to provide a complete suite of Lagrangian statistics that describe the mixed layer currents and their variability based on a very extensive set of observations spanning many seasons. These characterizations of mean currents, eddy kinetic energies, time and length scales, and spreading rates should be useful to numerical modelers who require such statistics to parameterize and validate global ocean circulation models.

This thesis is organized as follows: in Section II the drifter is described together with the temporal and spatial extent of the data from the SUBDUCTION region. Section III

provides velocity statistics as a function of region and season and as zonal averages. Section IV describes the Lagrangian statistics that give indications of time scales, length scales, diffusivities, and rotation preferences. Section V describes some of the eddies present in the data set and a new method for objectively locating eddies in drifter data by computing the radius of curvature of the trajectories. Conclusions and recommendations for further work are presented in Section VI.

## **II. DATA SET**

### **A. SATELLITE-TRACKED SURFACE DRIFTERS**

The instruments used consisted of ARGOS-tracked surface drifters with Holey Sock drogue elements. They were constructed according to specifications of the World Ocean Circulation Experiment's (WOCE) Surface Velocity Program (SVP; Sybrandy and Niiler, 1991). These drifters have a drag area ratio of 41. Figure 1 shows a scale drawing of the drifter illustrating the relative sizes of the surface and subsurface floats and the drogue element. The midpoint of the drogue element is 15 m below the water line. The surface float houses the antenna, ARGOS transmitter, batteries, and a through-hull sea surface temperature sensor. A drogue-on sensor that was mounted in the surface floats failed to produce useful data for this set of instruments. Therefore, no direct measure of whether the drogues remained attached or not is available. For the purposes of this study, drifter position data was treated as drogued data. Indirect evidence, such as the overall lack of downwind motion in the two-year data set, suggests that the drogues were in place during the whole period.

The drifters were remotely tracked using the ARGOS system, which is flown on two NOAA<sup>1</sup> polar-orbiting satellites. Each satellite is capable of making its own determination of drifter position each time the drifter is in view of the sensors for a sufficient length of time (on the order of minutes). The Doppler shift of transmitter frequency with time observed by the satellite, together with accurate knowledge of the satellite's position, places the drifter within a half cone of possible locations with the satellite at the apex of the cone. The intersection of that location cone with the ocean surface limits the possible locations to just two positions symmetrically located with respect to the satellite ground track

---

<sup>1</sup> National Oceanographic Atmospheric Agency—NOAA

(Figure 2). Prior known locations plus a range of realistic drifter velocities is used to resolve the final ambiguity.

Error in drifter position data arrives from two sources: 1) error in the positions derived from the ARGOS system as described above and 2) error due to slippage of water past the drogue element. This latter error is discussed in the next section. Errors in the ARGOS positions themselves are well documented. The operators of the system specify the accuracy of position fixes in terms of the standard deviation of positions about a known point. This means that, assuming a normal distribution of the error, 68% of the calculated values fall inside a radius equal to the standard deviation from the real position. Each fix includes an indicator of the position confidence based on the length of time the satellite was able to track the drifter on the ocean surface. These indicators (classes) are 1, 2, or 3. The standard deviations for these classes are 1000 m, 450 m, or 150 m, respectively.

The data in this study derived from positions with a mixture of location classes. An opportunity to estimate the position accuracy and precision for the geographical location was given by a drifter which apparently stuck on land (São Jorge Island), or was abandoned on land. It continued to broadcast for over one year from the same location. The locations provided by the ARGOS system during this time are shown in Figure 3. The gridded nature of the points illustrates the maximum resolution of the data stream (43 m east-west and 60 m north-south). The standard deviations of the locations were 383 m in the east-west direction and 359 m in the north-south direction relative to the year-long mean position. These values provide the best measure of the ARGOS system position accuracy for the data set used in this study.

## **B. LAGRANGIAN NATURE OF THE DRIFTERS**

The second source of error in the drifter position data is caused by slippage of the water past the drogue elements. This is due to the effect of wind and waves on the surface float and tether components and to the effect of vertical shear on the drogue itself. For the particular drifters used in this study, field tests have been conducted to calibrate the slip past the drogue elements as a function of wind speed and velocity shear (Niiler et al. 1987;

1993). The calibration was accomplished by attaching current meters to the top and bottom of the drogue elements for various sizes of drogues under varying wind conditions. Niiler et al. (1993) present the best-fit model for correcting drifter motion as a function of wind speed, shear, and the drifter drag area ratio. For the Holey-Sock drifters used in this study, the velocity error due to slippage past the drogue element is less than 2 cm/sec for wind speeds up to 20 m/sec. For typical wind speeds the error due to slip is less than 1 cm/sec, which is comparable to the error of modern moored current meters (Weller and Davis, 1980). It is important to note that earlier-generation drifters with small drag ratios experienced significantly more error due to slip. The drifters used in this study are also quasi-Lagrangian tracers of water motion because they are confined to one level (approximately 15 m) and do not follow water motions in three dimensions. This two-dimensional aspect of the instruments does not, however, affect the study of horizontal currents.

## **C. OVERVIEW OF THE DATA RETURNED**

### **1. Spatial Coverage**

A summary of the spatial coverage obtained by the drifter data is presented in Figure 4, which shows the trajectories of all SUBDUCTION drifters during the period investigated in this study. Thirty-six separate drifters are represented in the figure. The trajectories are based on 2-day-interpolated positions. (The interpolation procedure is described below.) The drifter coverage extends over, roughly, a 1000 km x 1000 km portion of the northeast Atlantic Ocean between the Azores Islands and the Canary Islands. Figure 5 shows the number of 2-day drifter observations available as a function of either longitude or latitude. The distributions are peaked at a median longitude and latitude of 26.7° W and 33.1° N, respectively. Although the distributions are roughly symmetric about these median locations, it will be shown that the non-uniform nature of the data distribution may significantly effect average velocity statistics computed from the drifter data.

The initial deployment locations of the 36 drifters analyzed in this study are shown in Figure 6. All of these instruments were deployed by volunteer observing ships traveling, primarily, between Miami and Gibraltar. The deployment locations are scattered throughout the data area but there are also high concentrations along latitude lines on the northern and southern side of the climatological latitude of the Azores Front. This region of the front is referred to as the Frontal Zone (FZ). In subsequent analyses, drifter data is divided into regions as a function of latitude. Data from south of  $33^{\circ}$  N are classified in the "South" region and data from north of  $35^{\circ}$  N are classified in the "North" region. The Frontal Zone is considered to extend between  $33^{\circ}$  N and  $35^{\circ}$  N in the calculation of the basic statistics in Section III but it is extended to  $36^{\circ}$  N for the Lagrangian statistics presented in Section IV. This extension was necessary to get enough contiguous trajectories in the Frontal Zone to compare with trajectories from the South and North regions. The delineation of the South, North and Frontal Zone regions are shown on Figure 6.

Mesoscale eddies are reflected in the drifter trajectories of Figure 4. Despite this eddy activity, the striking part of the trajectory data is that very few drifters moved out of the area of the Canary Basin, even though they drifted within the region for up to two years. This is in sharp contrast to observations based on earlier-generation drifters that were less effective water followers. They were observed to rapidly transit this area traveling southwestward in the climatological direction the winds (Krauss and Käse, 1984).

## **2. Temporal Coverage**

The drifters were released at different times during the experiment. They were generally deployed in groups of 4 or 5 from the volunteer ships. The temporal extent of each of the drifters is shown in Figure 7. The deployment groupings of 4 or 5 drifters are clearly visible in the figure. Many of the instruments operated for a very long period with 16 drifters operating for at least 15 months. At the end of the study period (31 May, 1993), twenty-four drifters were still operating.



In subsequent analyses, drifter data is divided into seasonal groupings in a manner similar to that described for the regional groupings by latitude. The number of 2-day observations available in each month is shown in Figure 8a. A continuous increase in available data is seen for the first 9 months, after which the number of 2-day observations available is roughly constant at around 1800. The seasonal grouping of data was actually done by combining data for a given season from all available years. Figure 8b, shows the number of available 2-day observations by month where multiple years have been combined. A fairly uniform number of observations is available for each month except for the month of June, which is under-represented because the observations used in this study began in July 1991 and ended in May 1993. The seasonal groupings were defined as three-month periods and referred to as winter, spring, summer, and fall. The definitions by month and year day from the beginning of 1991 are presented in TABLE I. The data set covers two seasons for each of the 3-month-long seasonal divisions used in the study.

#### **D. CONSIDERATION OF THE TRANSMITTER DUTY CYCLE**

The utility of drifting buoy measurements as used in this study derives from the large number of independent velocity samples that can be obtained for a reasonable cost. Although the technological trend since the advent of satellite-based tracking has been toward less expensive and longer lived drifters, the tracking costs of the ARGOS system—as it has been operated to date—have remained relatively high. The cost to track one drifter for one full year is approximately \$4000, which is larger than the, approximately, \$3000 cost of the instruments themselves. In order to reduce tracking costs, the transmitters in these drifters were programmed to operate for 24 hours and then stop operating for 48 hours. This transmission schedule incurs charges of one third the full-on rate (approximately \$1300/year) at the expense of higher frequency observations of the surface currents.

**TABLE I. YEAR DAYS DURING THE EXPERIMENT (1096 DAYS) COUNTING FROM 1 JANUARY 1991. SHADED AREAS IN 1991 ARE PERIODS WITHOUT DATA AND THE SHADED AREA IN 1993 WAS NOT INCLUDED IN THIS STUDY.**

<b>SEASONAL DIVISION</b>			
	<b>1991</b>	<b>1992</b>	<b>1993</b>
<b>WINTER</b> (JAN - MAR)	1 - 90	366 - 456	732 - 821
<b>SPRING</b> (APR - JUN)	91 - 181	457 - 547	822 - 912
<b>SUMMER</b> (JUL - SEP)	182 - 273	548 - 639	913 - 1004
<b>FALL</b> (OCT - DEC)	274 - 365	640 - 731	1005 - 1096

During the day in which the drifter transmitters operate, several location fixes are typically received. Figure 9a shows a histogram of the number of locations per day during the days when the transmitters were operating for the entire SUBDUCTION drifter data set. Typically, eight position fixes are received during a 24-hour period when the transmitters are operating. Figure 9b shows a histogram of the time separation between fixes for the entire data set. The time between fixes is usually less than 6 hours. The most common separation is 1.5 hours. The peaks in the histogram for time separations around 48 hours are due to the preprogrammed 48-hour shutdown mode. Even though several locations per day are received when the transmitter is on, it is only possible to resolve motions with periods greater than 48 hours due to the large gaps in the location data. All analyses in this study are confined to periods greater than 96 hours. This excludes, for

example, motions at the inertial period, which is about 15 hours at the latitudes of this study.

## **E. DESCRIPTION OF THE INTERPOLATION PROCEDURES**

Many of the statistical analysis performed in this study require evenly-sampled time series. The unprocessed data set obtained from the ARGOS system consists of irregularly-spaced position data for each drifter. The first step in the data processing was to remove positions that produced an inferred drifter velocity greater than 1 m/sec. After removing obviously bad points in this way, evenly-spaced time series were prepared using a method that combined linear and cubic spline interpolation. Spline interpolation has the advantage of preserving more information about the curvature in the drifter trajectory. Spline interpolation can produce quite bad results, however, when there are large gaps in the original data. An example of the pathological behavior of spline interpolation is shown in Figure 10, which shows the locations of the original data from the ARGOS system, together with 2-day linear and spline interpolation estimates for a segment of the trajectory for drifter number 14437. For most estimates the spline interpolation is very close to the original data and to the linear interpolation estimate. In one case, near  $15.4^{\circ}$  W,  $33.0^{\circ}$  N, the spline interpolation estimate is clearly quite far off from the data. At the same time, the linear interpolation estimate is much better.

In order to develop a scheme that uses cubic spline interpolation when possible and linear interpolation at other times, the difference in longitude and latitude for spline interpolated and linear interpolated position estimates was compared for the entire drifter data set. Figure 11 shows a histogram of the results. In the vast majority of cases the two estimates are within  $0.1^{\circ}$ . A hybrid or mixed interpolation scheme was adopted that used the spline interpolated estimate except where the difference between spline and linear estimates was greater than  $0.1^{\circ}$ . Longitude and latitude time series were analyzed separately for each drifter. As an example, the result of the mixed interpolation scheme is also shown on Figure 10. The bad spline highlighted above was replaced by the linear interpolation estimate in the mixed interpolation scheme.

Horizontal velocity estimates were produced for each drifter by center differencing the 2-day-interpolated position data. Longitude and latitude data were converted into kilometers east and west of the average drifter position before the velocity calculations were made. The final processed data set for this study was observations of position and horizontal velocity every even day for each of the 36 drifters. These data were used to obtain the statistical descriptions presented in the following sections.

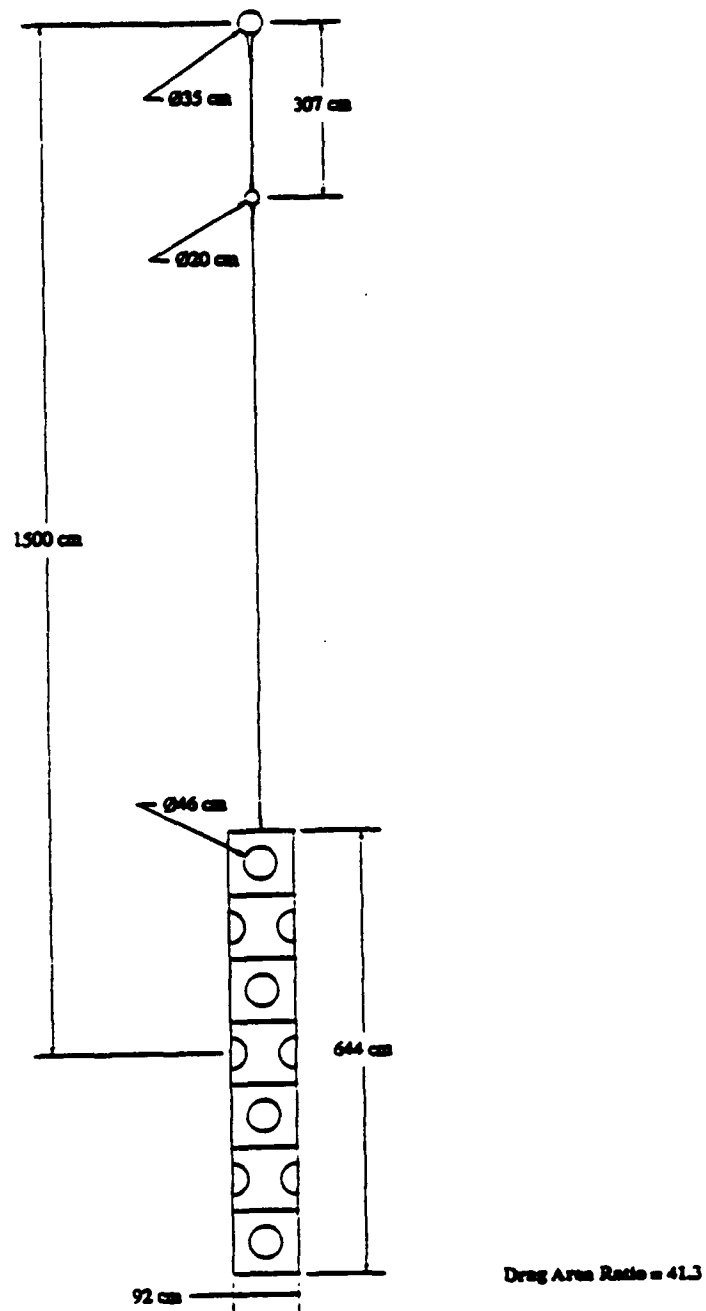


Figure 1. Scale drawing of the Holey Sock drifting buoy.

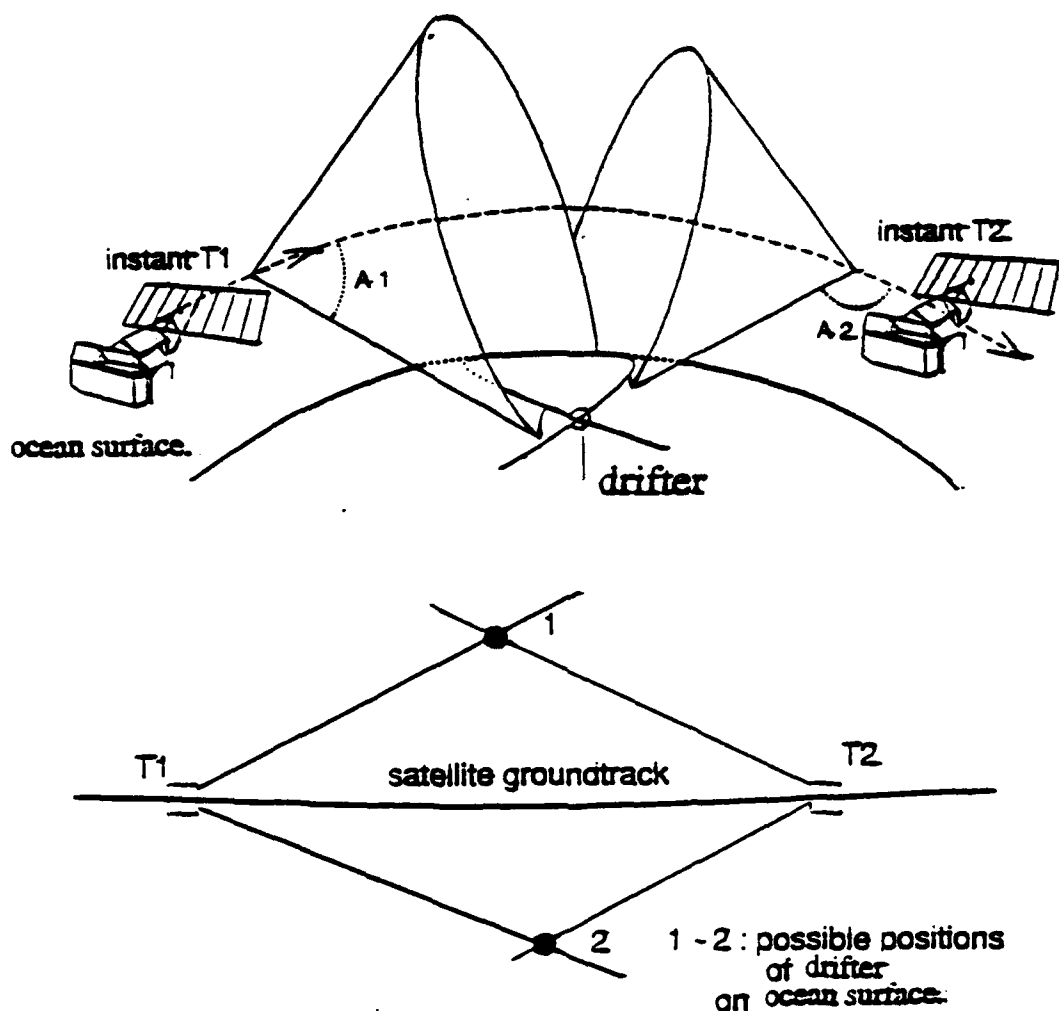


Figure 2. Drawing illustrating the principal of buoy positioning using the ARGOS system. The ARGOS sensors monitor the Doppler frequency shift of the transmitter on the surface buoy. Knowledge of the satellite position determines the possible buoy positions at the intersections of the range cone and the ocean surface.

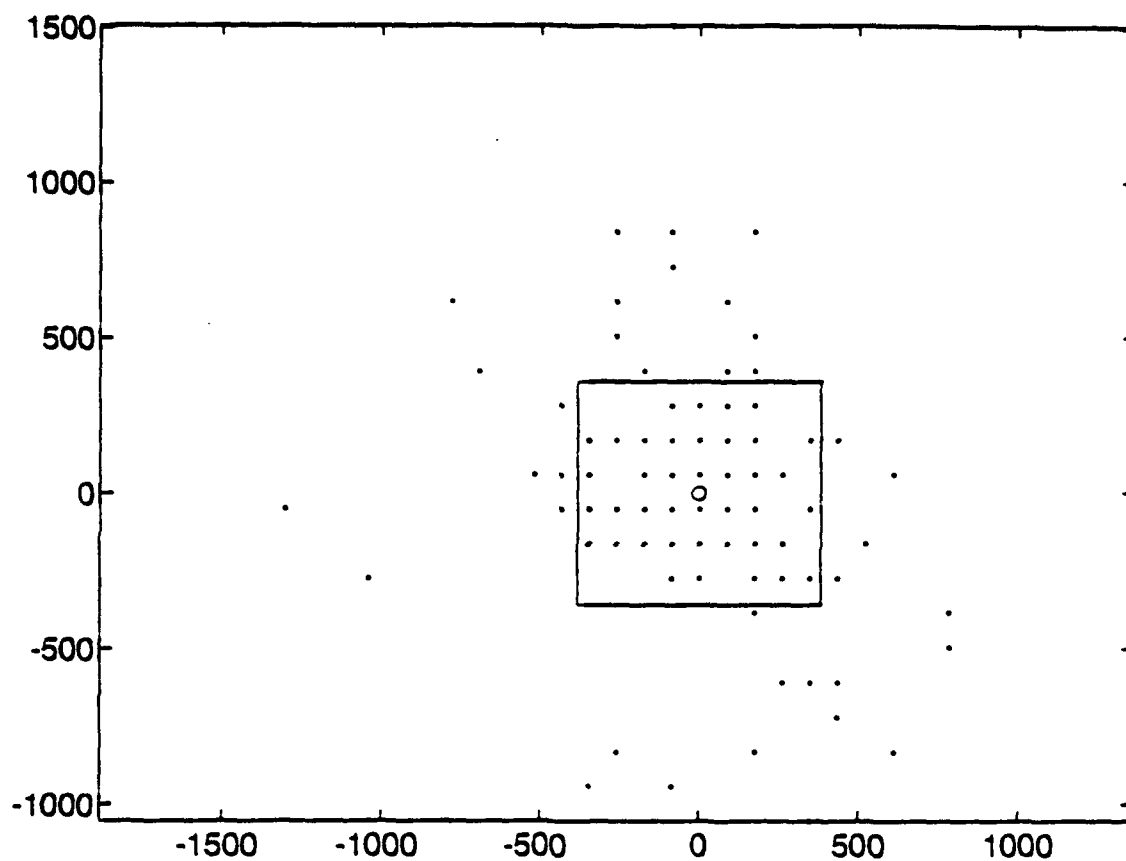


Figure 3. Locations of buoy 14458 in kilometers east and north of its mean position after grounding on São Jorge Island (o). The spacing of the points shows the maximum resolution of the position data. The box shows the standard deviation of the reported positions.

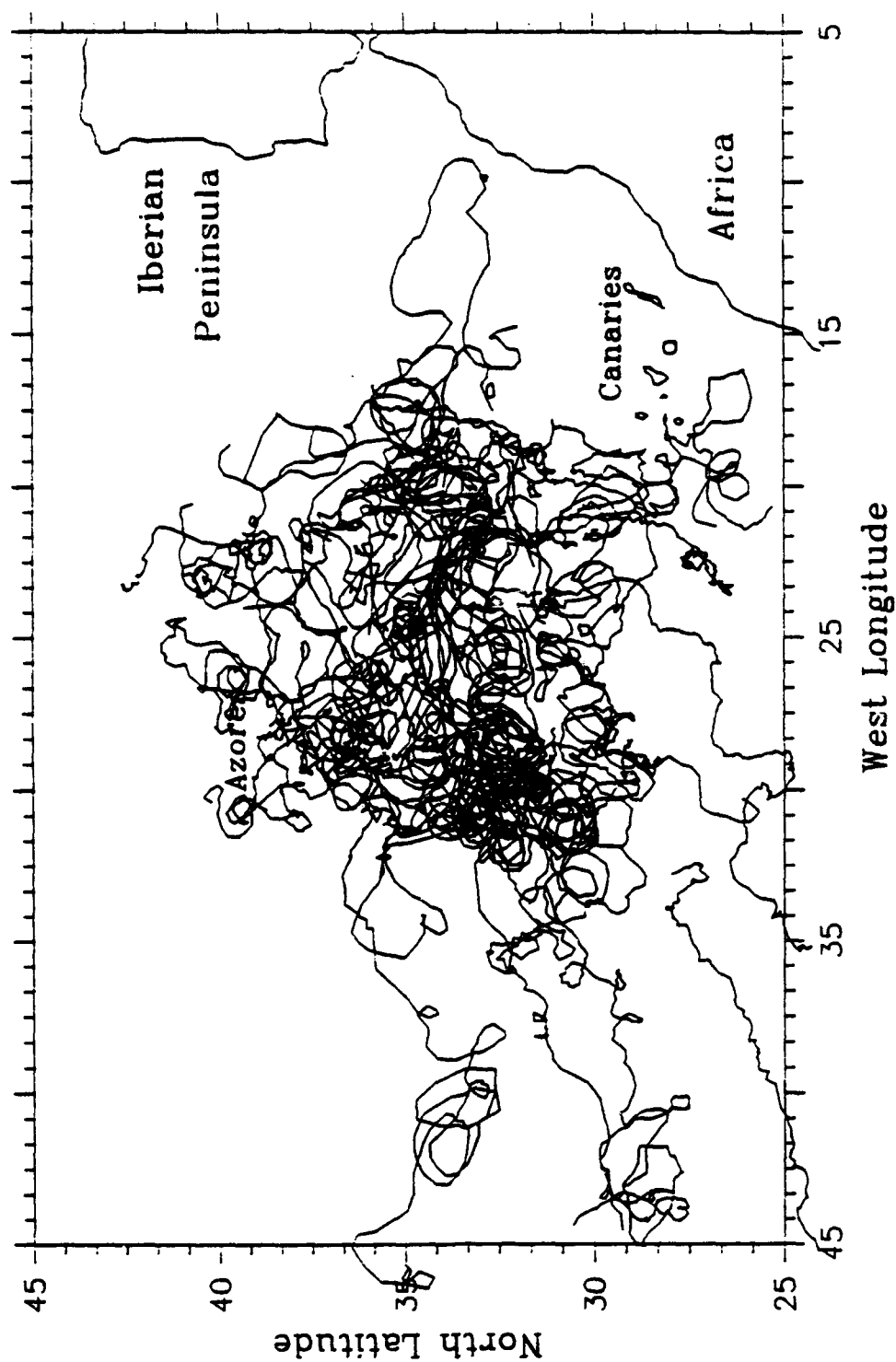


Figure 4. Trajectories of 36 surface drifters for the period from July 1991 through May 1993. Positions derive from the 2-day-interpolated data set.



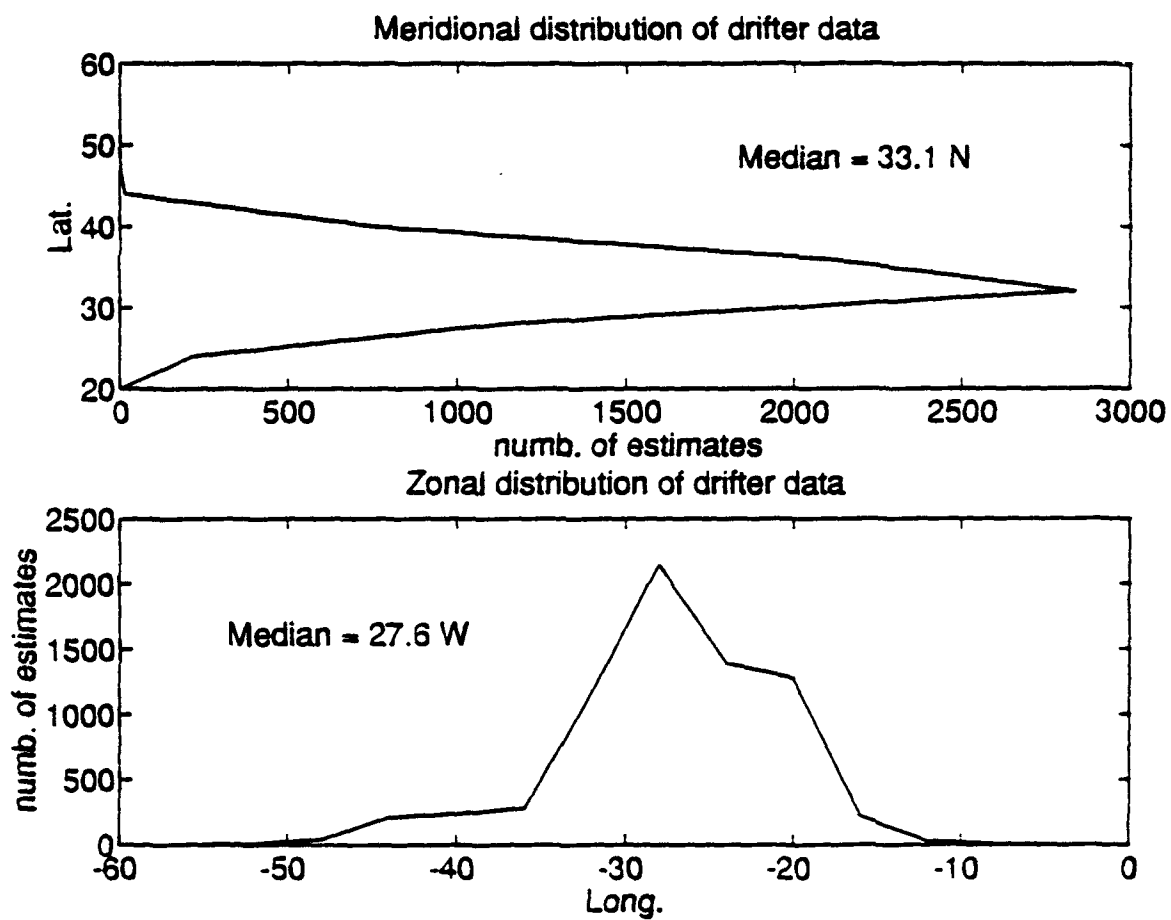


Figure 5. Number of 2-day-interpolated positions or velocity estimates from the surface drifter data set as a function of latitude (upper panel) and longitude (lower panel).

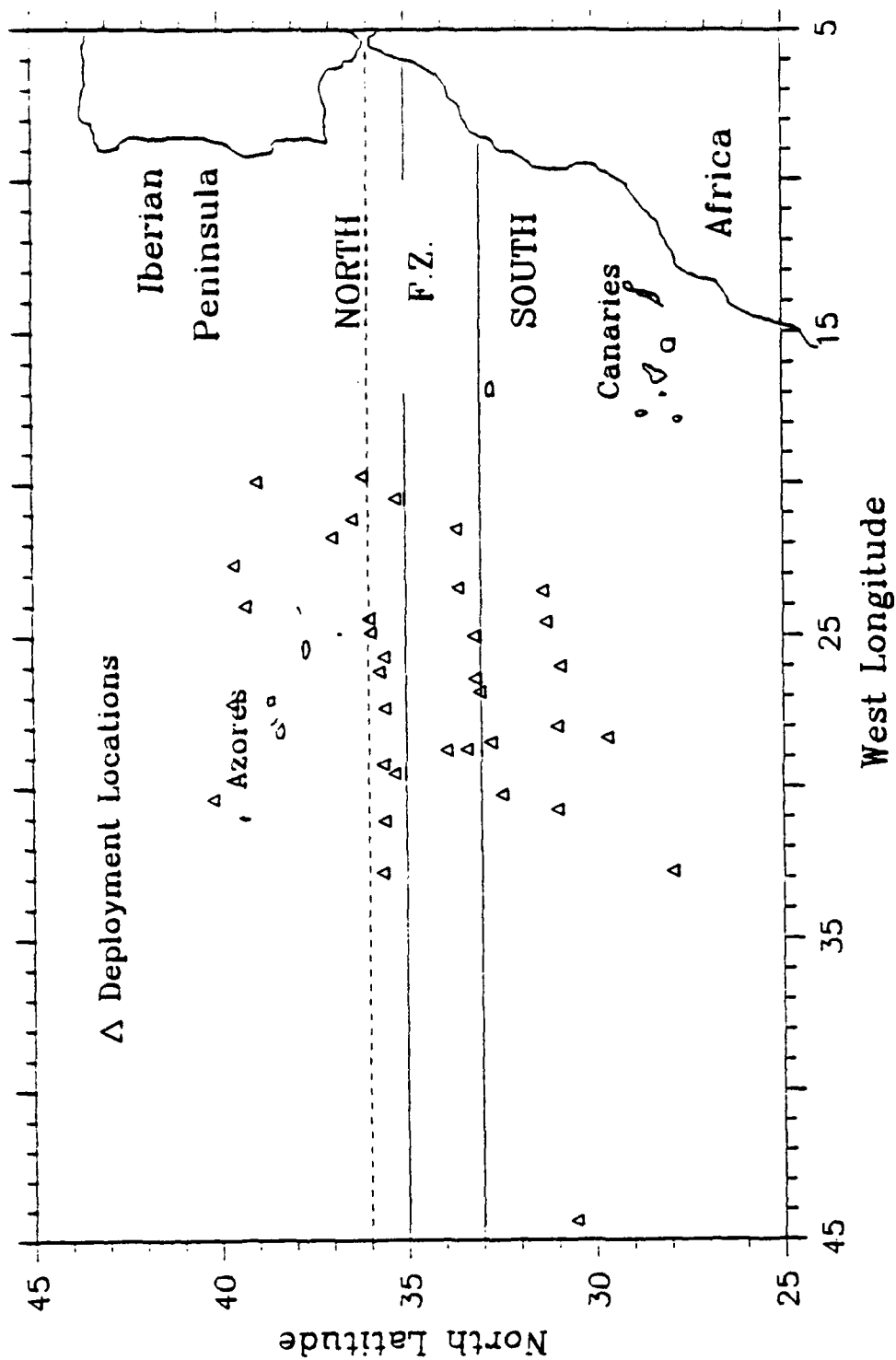


Figure 6. Initial deployment positions of surface drifters (symbols). The boundaries for regions used to compute zonally-averaged statistics are also shown.

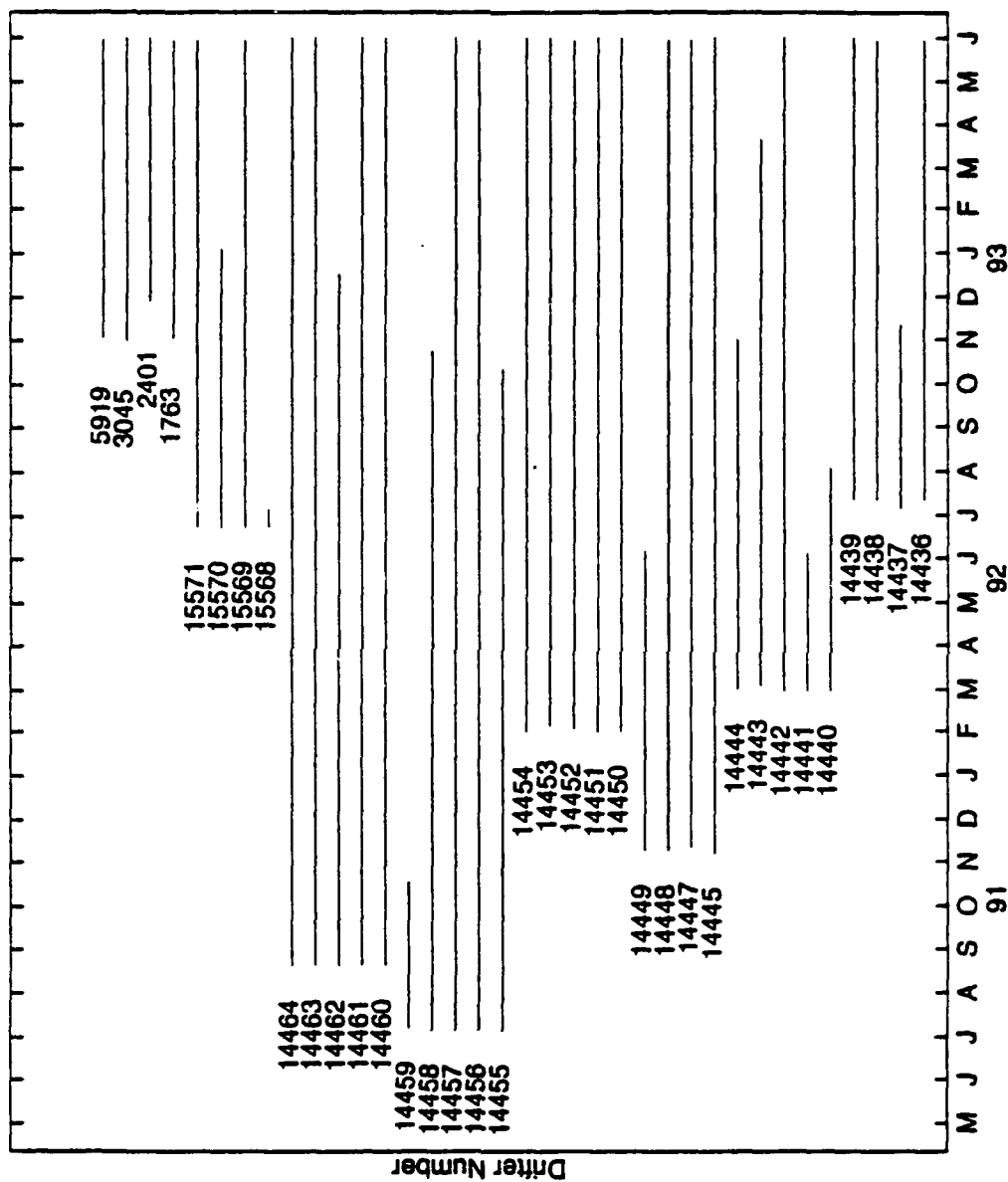


Figure 7. Time line of drifter performance. Numbers are the ARGOS identification numbers. Drifters extending through May 1993 were still in operation at the time of this study.

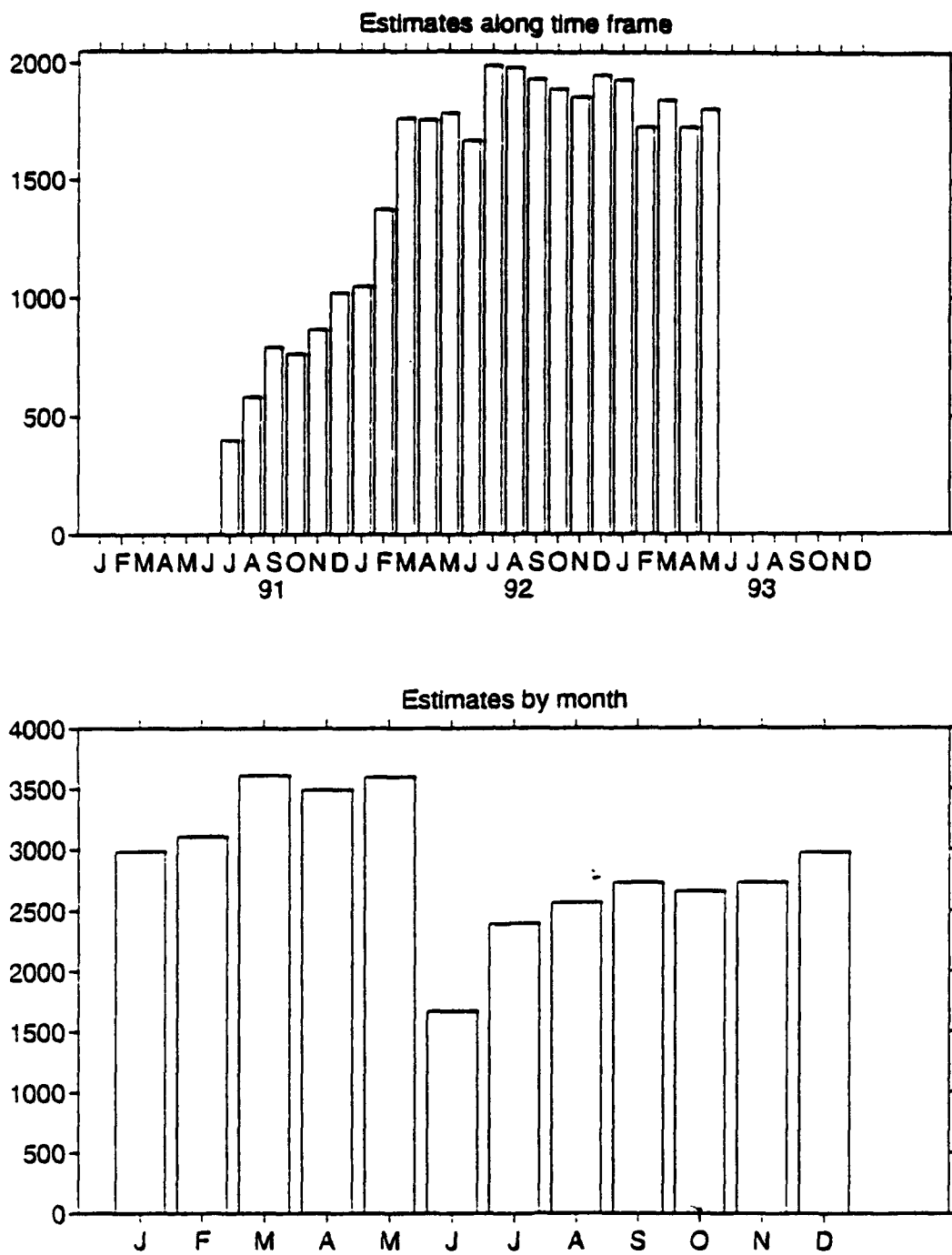


Figure 8. Histograms of the number of 2-day-interpolated position or velocity estimates available by month for individual months (a) and for combined months (b).

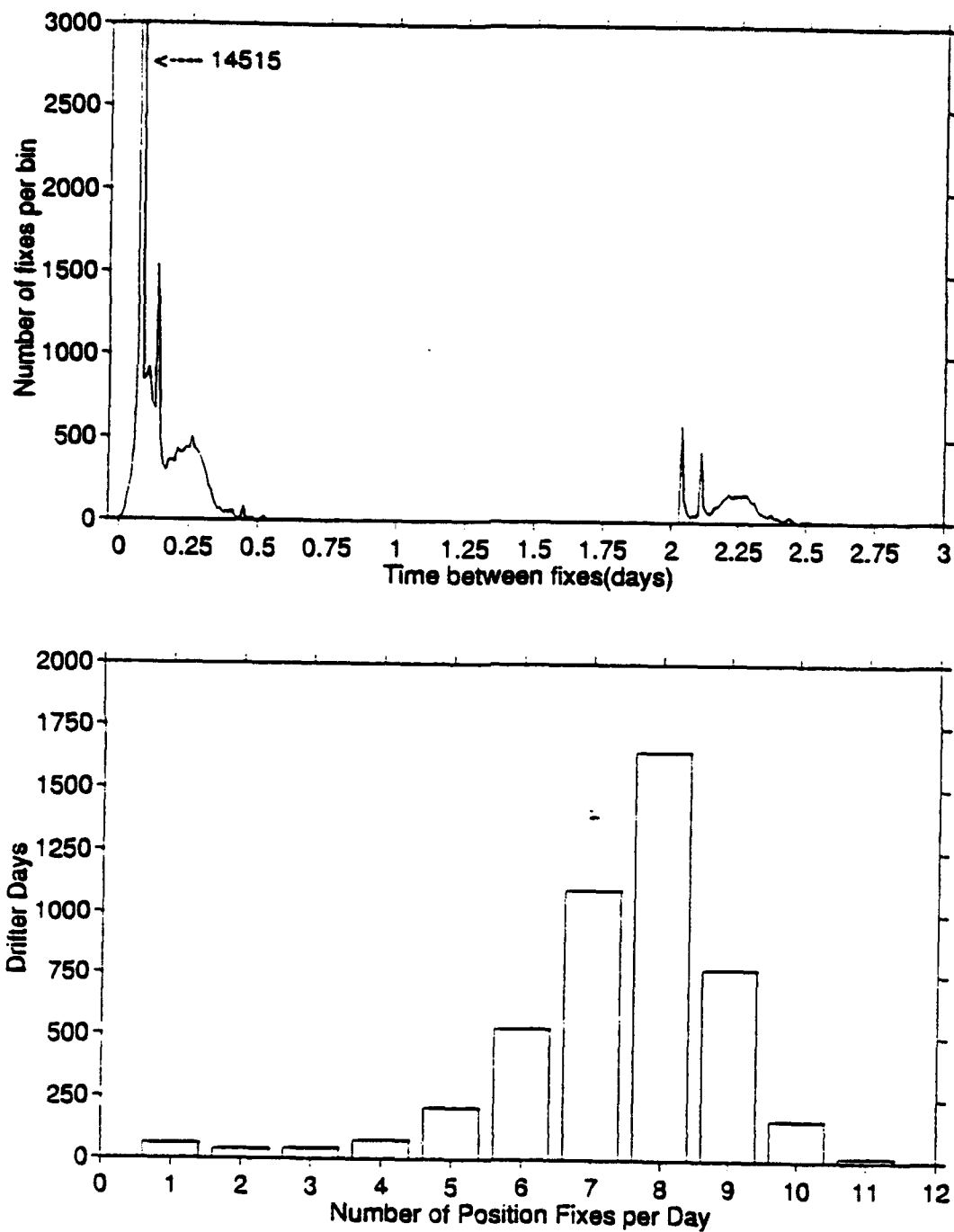


Figure 9. Histogram of the number of position returns per day when transmitters are operating (lower panel) and the time separation between position fixes for all drifters (upper panel). The time separations around 48 hours are due to the 1-day-on, 2-days-off duty cycle of the transmitters.

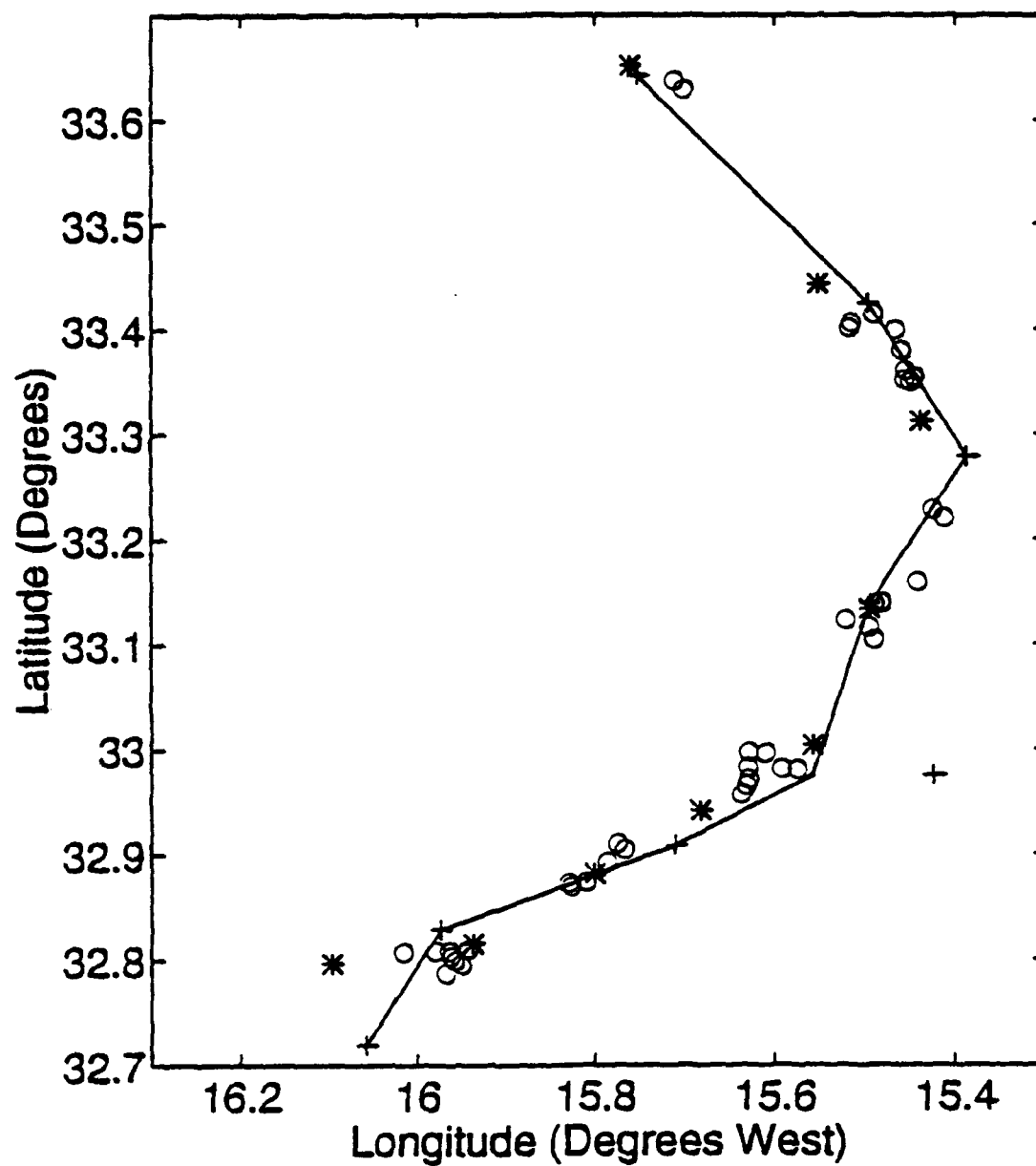


Figure 10. Partial trajectory from drifter 14437 showing original data (o), linear interpolation at 2-day intervals (\*), spline interpolation at 2-day intervals (+), and the result of the mixed linear and spline interpolation (solid line).

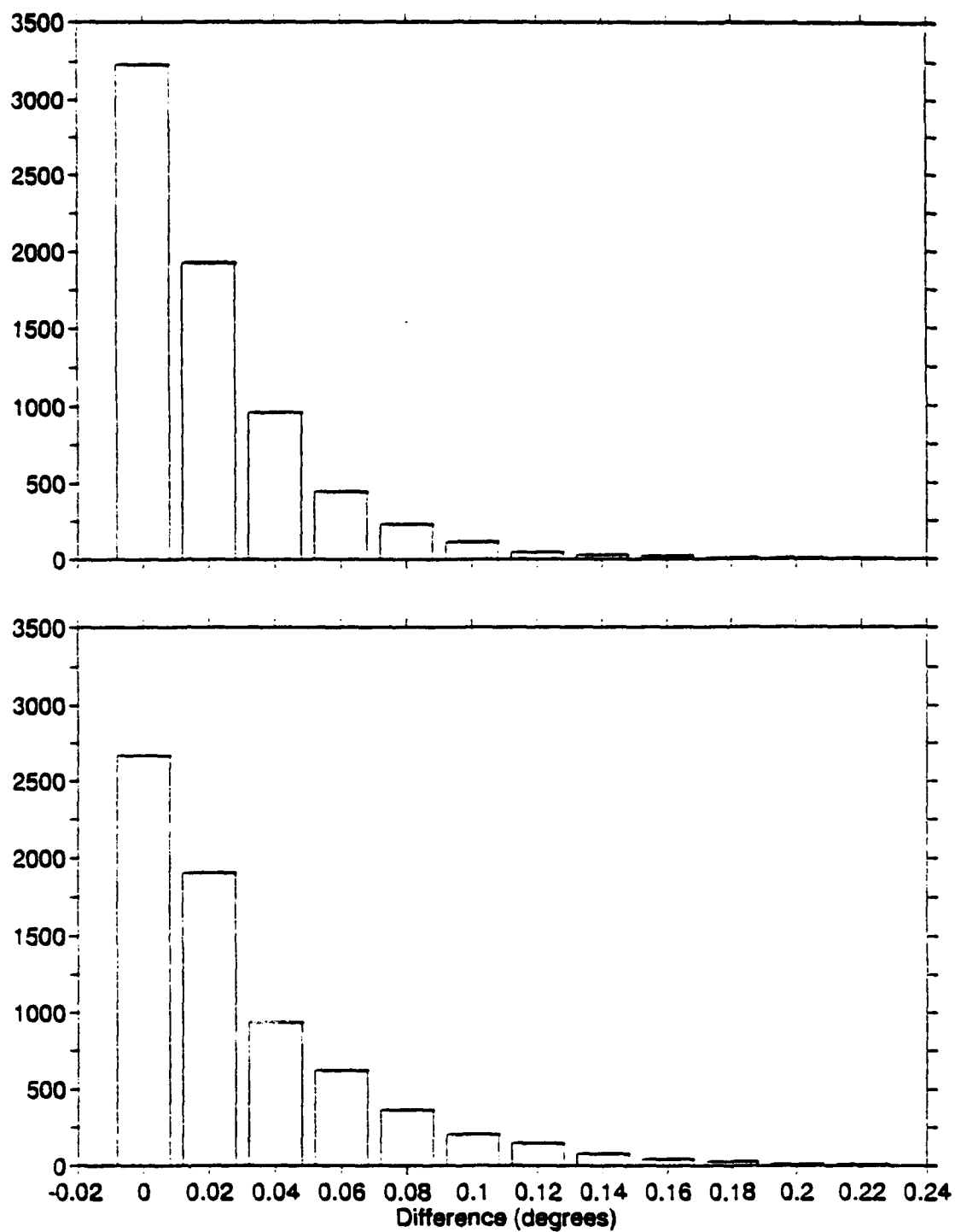


Figure 11. Histogram of difference between linear and spline interpolation in longitude (lower panel) and latitude (upper panel) for all 2-day-interpolated positions.

### III. BASIC STATISTICS

One of the goals of the drifter observations in the region of the SUBDUCTION Experiment is to measure the convergence of the mixed layer currents. This convergence is expected because of the climatologically-convergent Ekman transport in the area. The primary contribution to wind stress curl in the area comes from north-south variability of the east-west wind stress. Hence the dominant convergence in the mixed layer is expected to be in the north-south currents. It is also expected a priori that mean currents in the SUBDUCTION region are much weaker than the currents due to mesoscale eddies. Because of this, large numbers of observations are required to obtain a statistically-significant measure of mean currents.

In all cases zonal averages were used wherever regional divisions were made. This reflects the intended focus on in the north-south direction. Averages were also formed by time of year (TABLE I). These seasonal averages did not take account of location because there is not yet enough data in the SUBDUCTION region to perform separations by both season and location. The regional averages were computed in two ways: 1) by combining data for the entire range of longitudes in large areas covering many degrees of latitude (large area averages) and 2) by combining data for the entire range of longitudes in successive latitude bands extending over 1 degree of latitude (zonal averages). In the former case, three large regions were defined: the South region, which combined all data south of 33° N, the North region, which combined all data north of 35° N, and the Frontal Zone (FZ), which combined all data in the latitude range between 33° N and 35° N (Figure 6). The South region, FZ, and North region accounted for 48, 21, and 31 percent of the data, respectively.

In this section, the mean mixed layer velocity components ( $\bar{u}$ ,  $\bar{v}$ ) and their standard errors are presented for the entire data set and by large regions as functions of the number of 2-day-interpolated velocity estimates available since the beginning of the experiment. It is also possible to compute average velocities and standard errors for the ensemble of



drifters available each day or month or season, etc. For all mean current estimates the drifter data were treated with an Eulerian perspective. i.e. the data were combined according to the time and location of the observation without considering the trajectories from which they were derived. The exception to this is the estimation of standard errors of the means. To perform those calculations, it is necessary to know the number of *independent* velocity estimates that went into a particular average. That number was obtained by dividing the number of 2-day-interpolated velocity samples by the number of samples required to total one integral time scale. A, conservative, value of 10 days was used for the integral time scale, which is justified by the Lagrangian statistics presented in Section IV.

All averages presented in this thesis are accompanied by the 95% standard error of the mean, which is calculated according to the following formula:

$$\frac{2\sqrt{\sigma^2}}{\sqrt{N^*}} \quad (1)$$

where  $\sigma^2$  is the variance of the data and  $N^*$  is the number of independent observations. For example, in the case of the average velocity based on  $N$  2-day-interpolated observations,  $N^*$  is equal to  $N/5$ .

## A. LARGE AREA AND SEASONAL AVERAGES

### 1. Mean Currents

The cumulative mean values are presented in Figures 12 through 19 for the entire data set, regional averages, and the seasonal averages. In each figure, the mean eastward and northward velocity components are plotted against yearday. The computed averages are cumulative, however. That is, they are based on all available data from the time of the first observation until the yearday in question. The final values on each graph are, therefore, the mean values based on the maximum data available. Standard errors of the means are also shown as envelopes around the mean values. It should be noted that the

seasonal plots (Figures 16 through 19) contain horizontal segments connecting the seasons in consecutive years. Again, the very last values give the mean and standard error based on all observations fitting the particular seasonal window.

The most obvious result in the cumulative figures is the very low values for mean currents. After the first six months, the cumulative mean values settle down to less than 1 cm/sec in most cases. The final values for the entire data set and for each region and season are listed in TABLE II along with the final standard errors. The only significant mean values are found in the regional averages. In particular, the Frontal Zone has strong mean eastward currents of 3.9 cm/sec. In the South and North regions, the mean eastward currents are -1.3 cm/sec (to the west). There is a statistically-significant mean northward current in the South region of -1.1 cm/sec (to the south) and overall there is a barely-significant mean northward current of -0.6 cm/sec (to the south). There are no statistically-significant mean currents in the seasonal averages nor are there any obvious seasonal patterns.

Convergence of the mean northward current in the SUBDUCTION area is not apparent in the results of TABLE II. This result is addressed more closely in the zonal averages below.

## **2. Kinetic Energy**

The strength of the variability about the mean currents observed in the drifter data is also a useful measure of the currents in this area. The large number of observations obtained in this study provide a good characterization of the current variances. This Eddy Kinetic Energy, EKE, which is defined as the average of the east-west and north-south variance, can be compared with values from other oceanographic regions and with values obtained from numerical models of ocean circulation.

TABLE II. AVERAGE ZONAL ( $\bar{u}$ ) AND MERIDIONAL ( $\bar{v}$ ) VELOCITY COMPONENTS AND THEIR STANDARD ERROR (S.E.) FOR ENTIRE DATA SET AND BY REGION AND SEASON. ZONAL ( $\overline{u'^2}$ ) AND MERIDIONAL ( $\overline{v'^2}$ ) VARIANCES AND THE NUMBER OF 2-DAY OBSERVATIONS (N) ARE ALSO SHOWN.

	$\bar{u}$ (S.E.) cm/sec	$\bar{v}$ (S.E.) cm/sec	$\overline{u'^2}$ cm <sup>2</sup> /sec <sup>2</sup>	$\overline{v'^2}$ cm <sup>2</sup> /sec <sup>2</sup>	N
<b>ALL DATA</b>	-0.28 (0.57)	-0.58 (0.50)	115.9	89.4	7028
<b>FALL</b>	0.82 (1.13)	-0.53 (0.99)	110.2	87.0	1745
<b>WINTER</b>	-0.54 (1.03)	-0.65 (0.97)	102.0	93.7	1954
<b>SPRING</b>	-1.04 (1.23)	-0.64 (1.04)	134.5	95.8	1760
<b>SUMMER</b>	-0.35 (1.20)	-0.54 (1.01)	112.3	80.4	1569
<b>NORTH</b>	-1.28 (0.90)	0.25 (0.85)	91.5	81.0	2224
<b>FRONT-ZONE</b>	3.91 (1.73)	-0.57 (1.44)	207.3	141.6	1373
<b>SOUTH</b>	-1.32 (0.71)	-1.14 (0.65)	86.4	72.2	3431

The variances about the cumulative mean values for the entire data set and for the large regions and seasons are shown in the lower panels of Figure 12 through 19. For comparison, the EKE and the Mean Kinetic Energy, MKE, are also plotted. The MKE is defined as the average of the squares of the mean velocity components. In all of the averages MKE is nearly zero, many times smaller than EKE. The average EKE is 102 cm<sup>2</sup>/sec<sup>2</sup> for the entire data set (cf variances in TABLE II). Krauss and Käse (1984) found a very similar average EKE of 100 cm<sup>2</sup>/sec<sup>2</sup> in the SUBDUCTION region. There is very little change in average EKE for the different regional or seasonal groupings. The exception is EKE in the Frontal Zone where the average is 174 cm<sup>2</sup>/sec<sup>2</sup>. Again this is consistent with the earlier computations of Richardson (1983) who calculated EKE distribution for 2° squares in the north Atlantic from satellite-tracked drifters and found EKE in excess of 200 cm<sup>2</sup>/sec<sup>2</sup> for the area 32°–34° W by 32°–34° N, which is within the Frontal Zone region of this study.

The average EKE obtained from this study is shown in TABLE III together with values from previous drifter observations in both the Atlantic Ocean and Pacific Ocean. The different values point out differences in the mesoscale eddy activity in the various regions. TABLE III also shows average diffusivities, which are related to EKE. The Lagrangian diffusivities for this study—and the relationship of diffusivity and EKE—are described in Section IV.

TABLE III: COMPARISON OF EKE AND AVERAGE DIFFUSIVITY (DIFF) FOR VARIOUS STUDIES USING DRIFTERS.

PROJECT <sup>1</sup>	YEAR(s)	AREA	AV LAT.	EKE cm <sup>2</sup> /sec <sup>2</sup>	DIFF 10 <sup>7</sup> cm <sup>2</sup> /s
OCEAN STORMS	87	NE Pacific open ocean	49° N	41	1.4
CTZ	88	NE Pacific coastal filaments	33° N	228	3.7
FRONTS	85,86,88	NE Pacific east. boundary	30° N	101	3.9
KIEL	81-84	NE Atlantic	35° N	91	2.9
SUBDUCTION (PRESENT WORK)	91-93	NE Atlantic open ocean	33° N	102	5.0

## B. ZONAL AVERAGES

The second type of regional average that was performed using the drifter data was based on zonal averages over smaller bands. Averages of all 2-day-interpolated velocity estimates spanning the range of longitudes and 1 degree of latitude were computed. The results for overlapping 1 degree latitude “windows” computed every 0.2 degrees are shown in Figure 20 for the latitude range from 26° N to 40° N. The overlapping serves to smooth the results as a function of latitude. The north-south variability of the mean currents based on the drifter data is highlighted in these results.

---

<sup>1</sup>Values taken from the following references: Paduan and Niiler (1993), Brink et al. (1991, ensemble 3), Poulain and Niiler (1989), and Krauss and Böning (1987, ensembles 1 & 2).

The zonally-averaged velocity components shown in Figure 20 represent the mean conditions based on observations over two years from 36 drifters as described in Section II. The "success" of the measurements—in terms of the goal to observe statistically-significant mean currents in the SUBDUCTION region—are mixed. Standard errors of the mean components are also shown in the figure and they indicate that uncertainties are large, even with the large number of observations in this data set. (The number of 2-day-interpolated observations in each zonal average is also shown in Figure 20.)

The east-west velocity component is relatively well resolved in the data set, particularly for the latitudes around the Azores Frontal Zone. The average eastward velocity shows a significant current to the east of about 5 cm/sec over a band from 33° N to 35° N with a peak of 7.5 cm/sec at 34° N. The standard errors are less than 2 cm/sec for this velocity component. The drifter observations have clearly isolated the mean eastward velocity in the region of the Azores Front. North and south of the frontal latitude band there are significant eastward mean currents of -1 cm/sec to -3 cm/sec (to the west), opposed to the direction of the maximum currents. This is consistent with hydrographic observations of the Azores Front (Stramma and Müller, 1989). The fact that velocities are oppositely-directed in the Frontal Zone means that averaging over fixed latitude ranges over multiple years—as was done in this study—will produce mean values that are much lower than instantaneous values near the front. Far to the south of the Frontal Zone near 27° N there are significant mean eastward currents of -5 cm/sec (to the west) in a narrow latitude band. These results derive from relatively few drifters, however (cf Figure 4).

The zonally-averaged north-south velocity component does not show significant mean flow anywhere in the latitude range investigated. That is, the standard errors of the means are larger than the mean values for this component. The magnitude of the mean northward velocity is less than 1 cm/sec for most of the latitude range investigated. Between 26° N and 30° N the value approaches -2 cm/sec (to the south) but this is still less than the standard error of about 3 cm/sec.

Given the large uncertainties in the mean north-south velocity components, any discussion of those mean currents could be unnecessary. There is, however, a quite

consistent pattern to the mean currents as a function of latitude. In fact, there is a consistent north-south divergence of the mean northward velocity components over almost the entire latitude range with the exception of a narrow range from  $37^{\circ}$  N to  $38^{\circ}$  N. This is in direct opposition to the expected result of mean convergence of the northward surface currents in the SUBDUCTION region. A possible explanation for this unexpected result comes from the uneven distribution of observations in the data set. It is possible to estimate the size of the error due to non-uniform concentrations of drifter measurements given a measure of the concentration and a measure of the random spread, or diffusion, of drifters within the variable flow field. The number of 2-day-interpolated observations versus latitude (Figure 20) provides a measure of the concentration. The Lagrangian diffusivity provides a measure of the spreading. This bias is estimated in Section IV following the presentation of the diffusivity. It will be shown to be of the order of the mean northward velocity components in Figure 20 and of the proper sign to account for the divergence present in the latitudinal distribution.

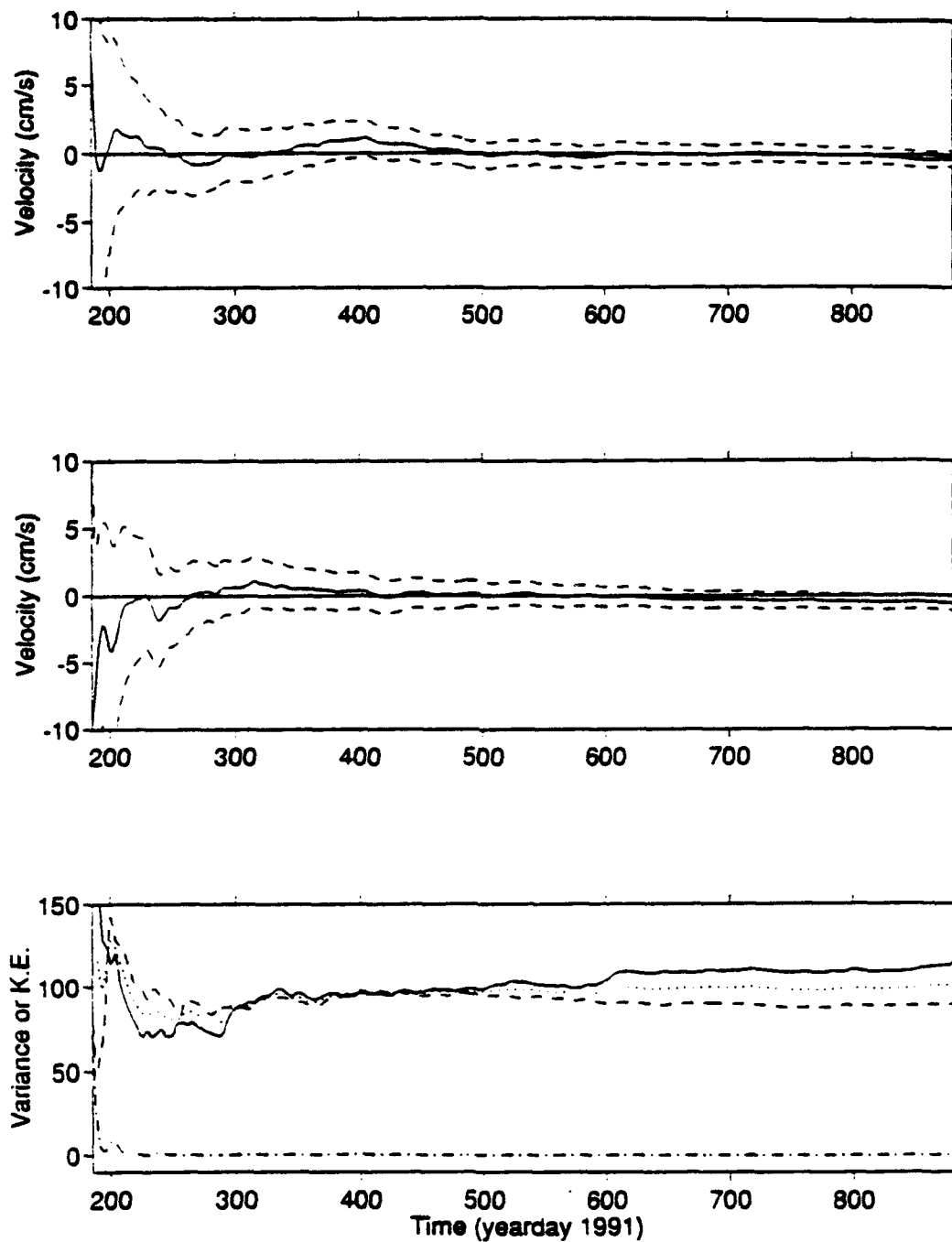


Figure 12. Average eastward (upper panel) and northward (middle panel) velocity (solid lines) and their standard errors (dashed lines) as a function of the cumulative number of 2-day-interpolated observations available since the beginning of the experiment. The eastward (solid) and northward (dashed) velocity variances are also shown (lower panel). The eddy kinetic energy (dotted) is shown for comparison with the very low mean kinetic energy (dashed-dot).

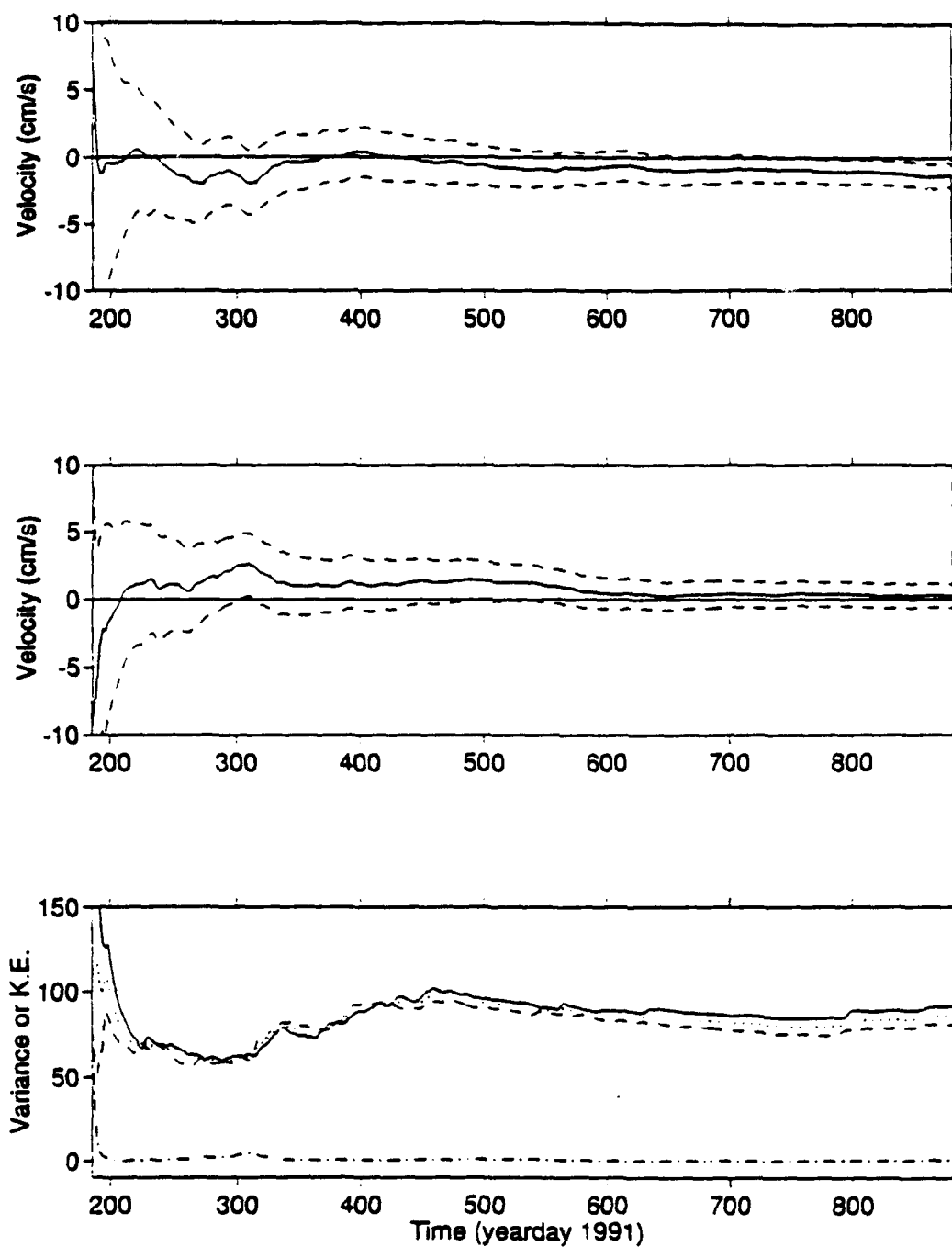


Figure 13. As in Figure 12 except for North region.



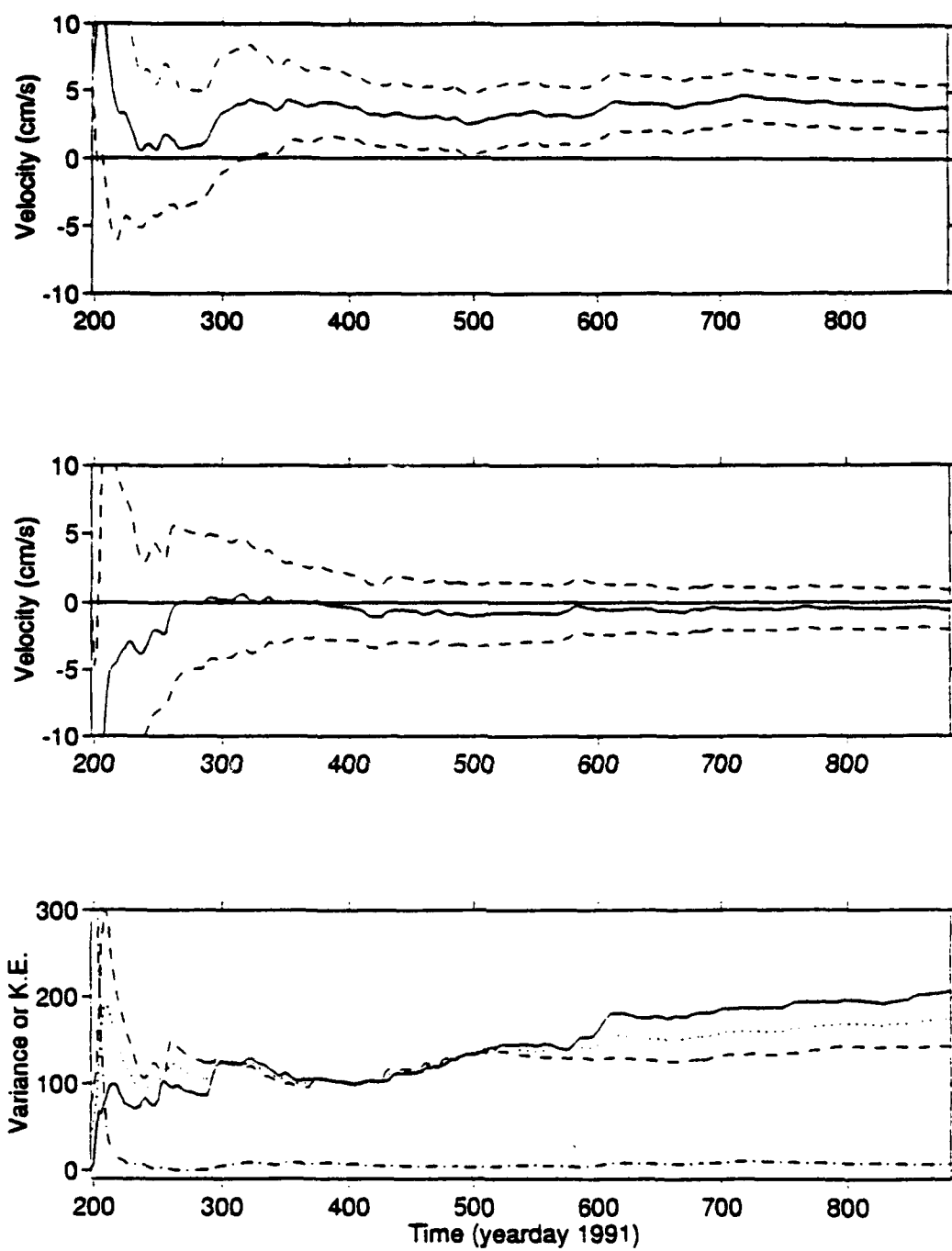


Figure 14. As in Figure 12 except for Frontal Zone. Note change in scale of lower panel.

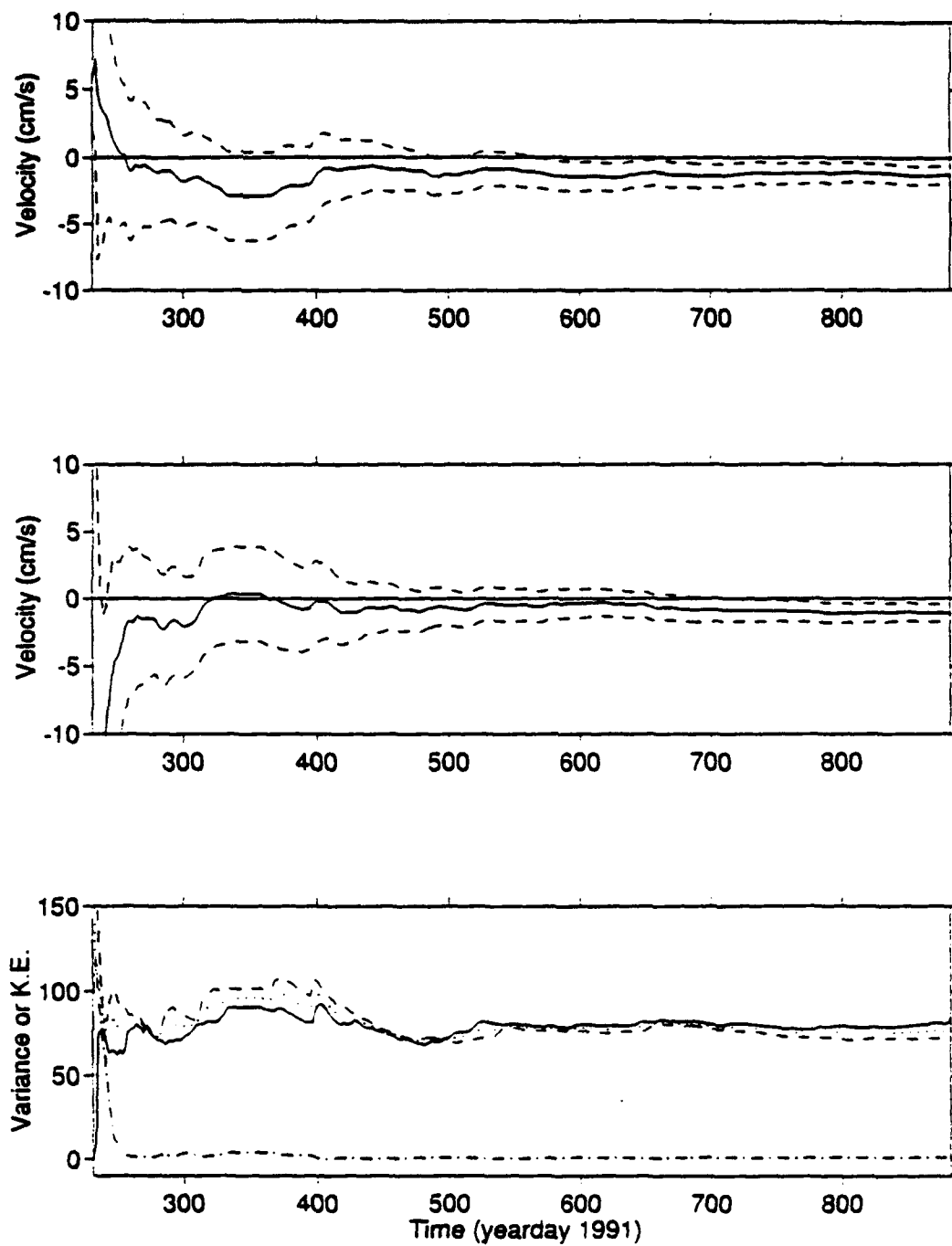


Figure 15. As in Figure 12 except for South region.

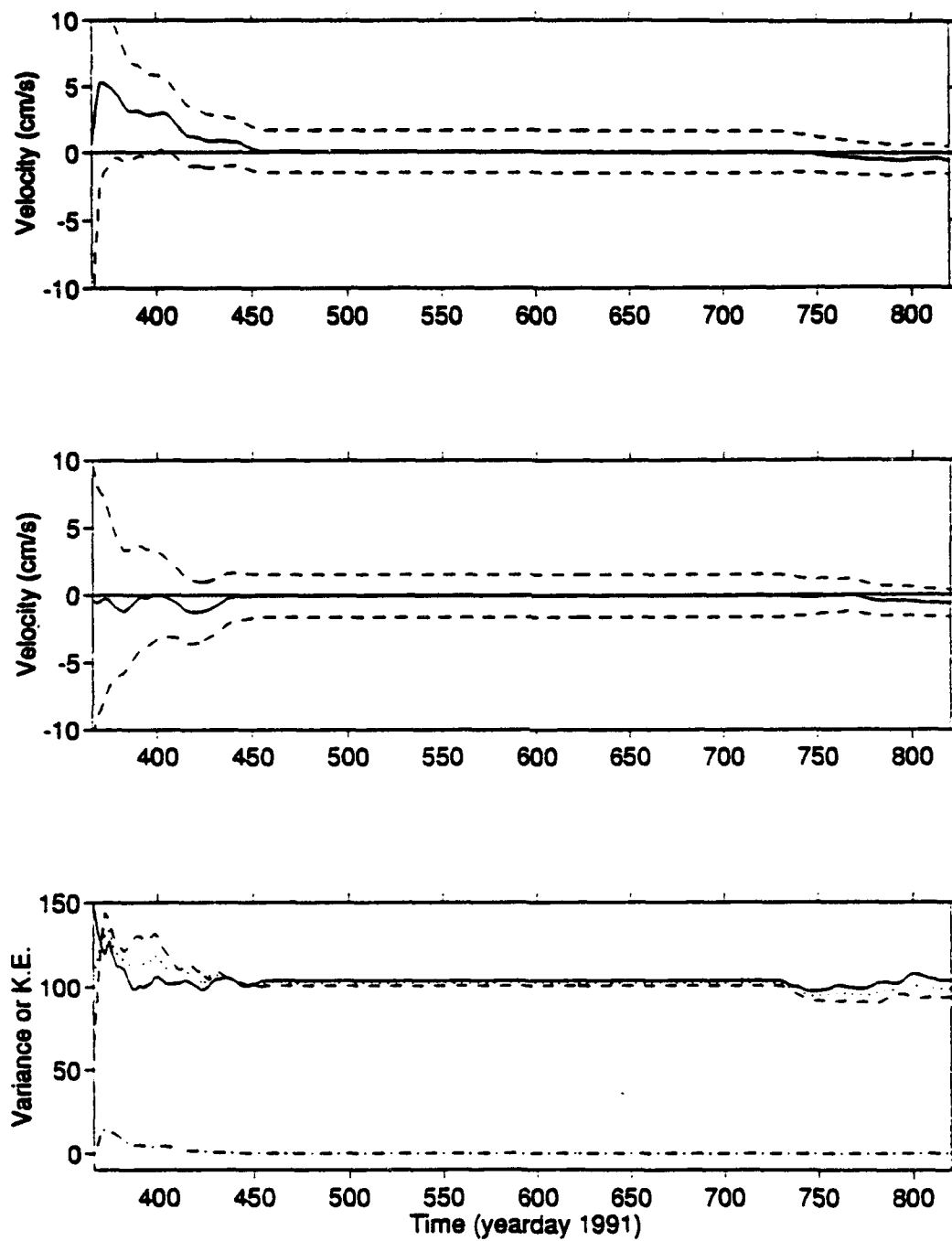


Figure 16. As in Figure 12 except for Winter data only.

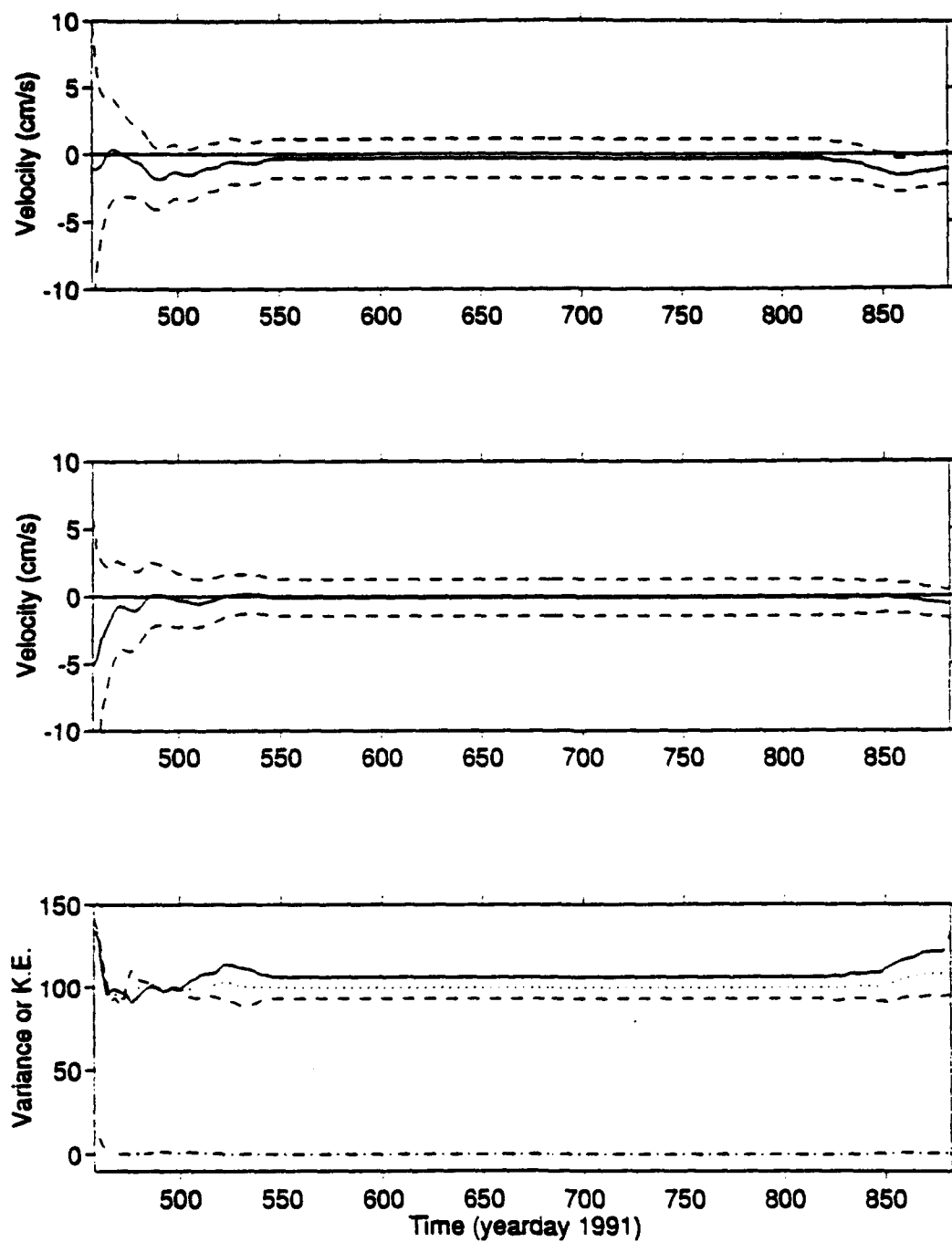


Figure 17. As in Figure 12 except for Spring data only.

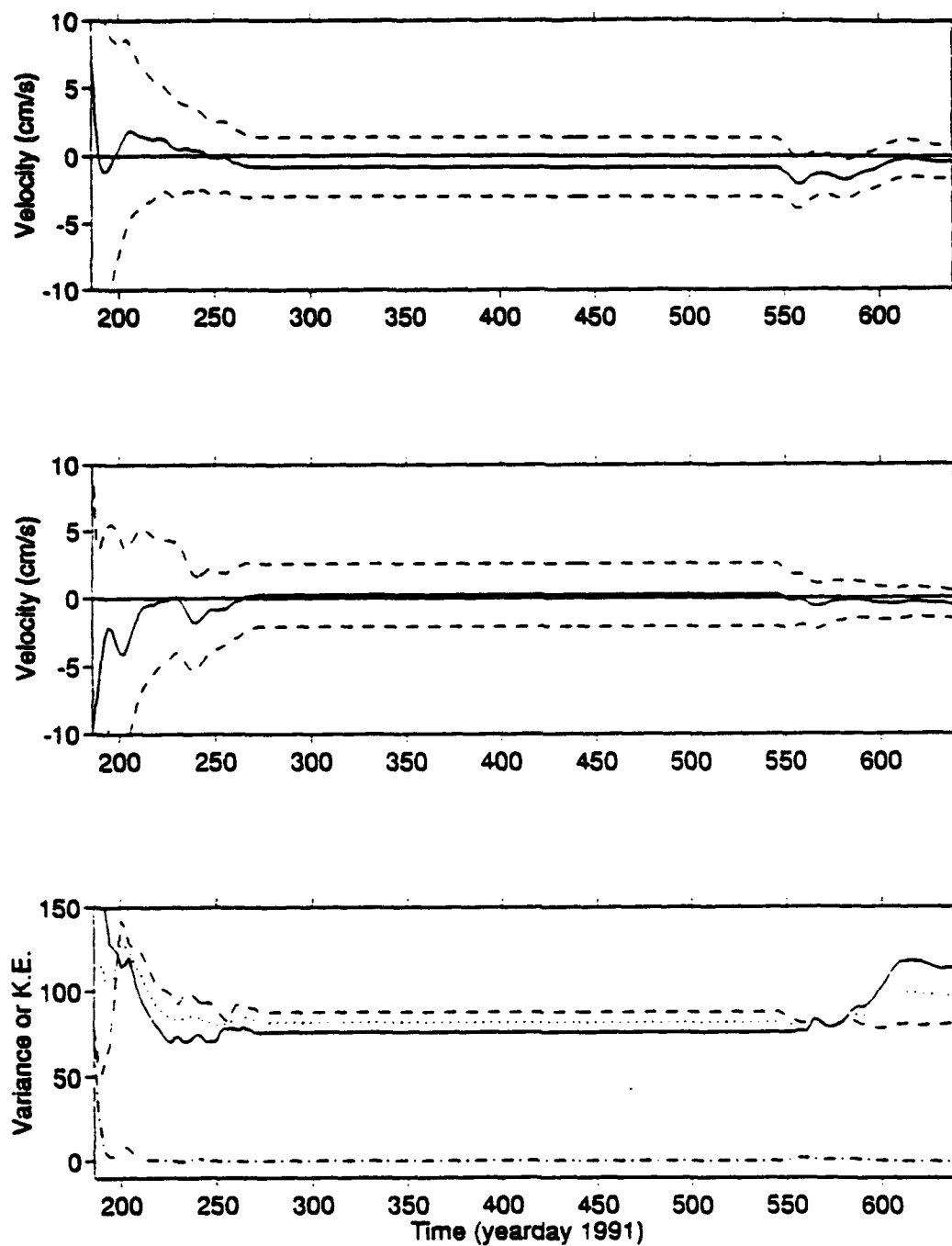


Figure 18. As in Figure 12 except for Summer data only.

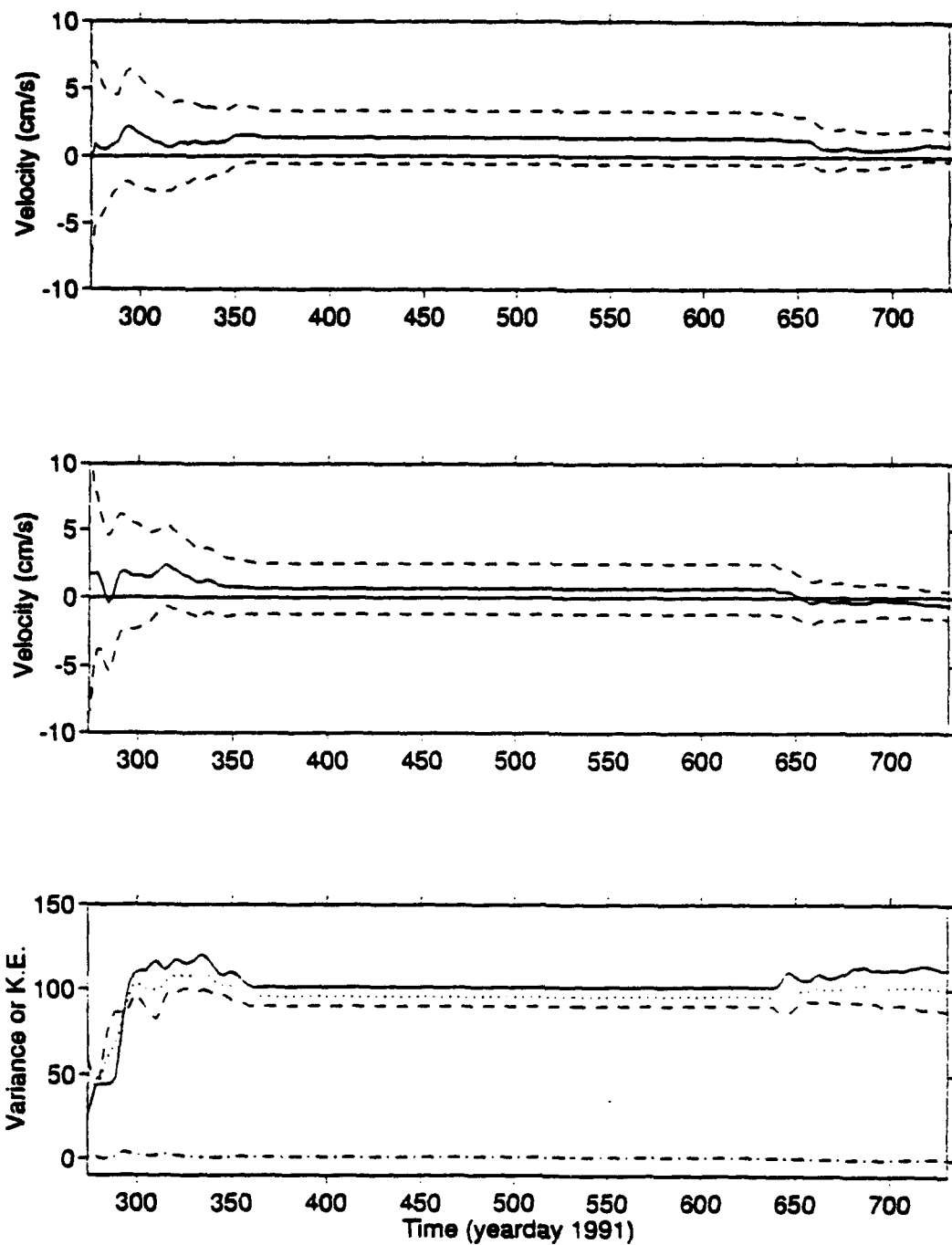


Figure 19. As in Figure 12 except for Fall data only.

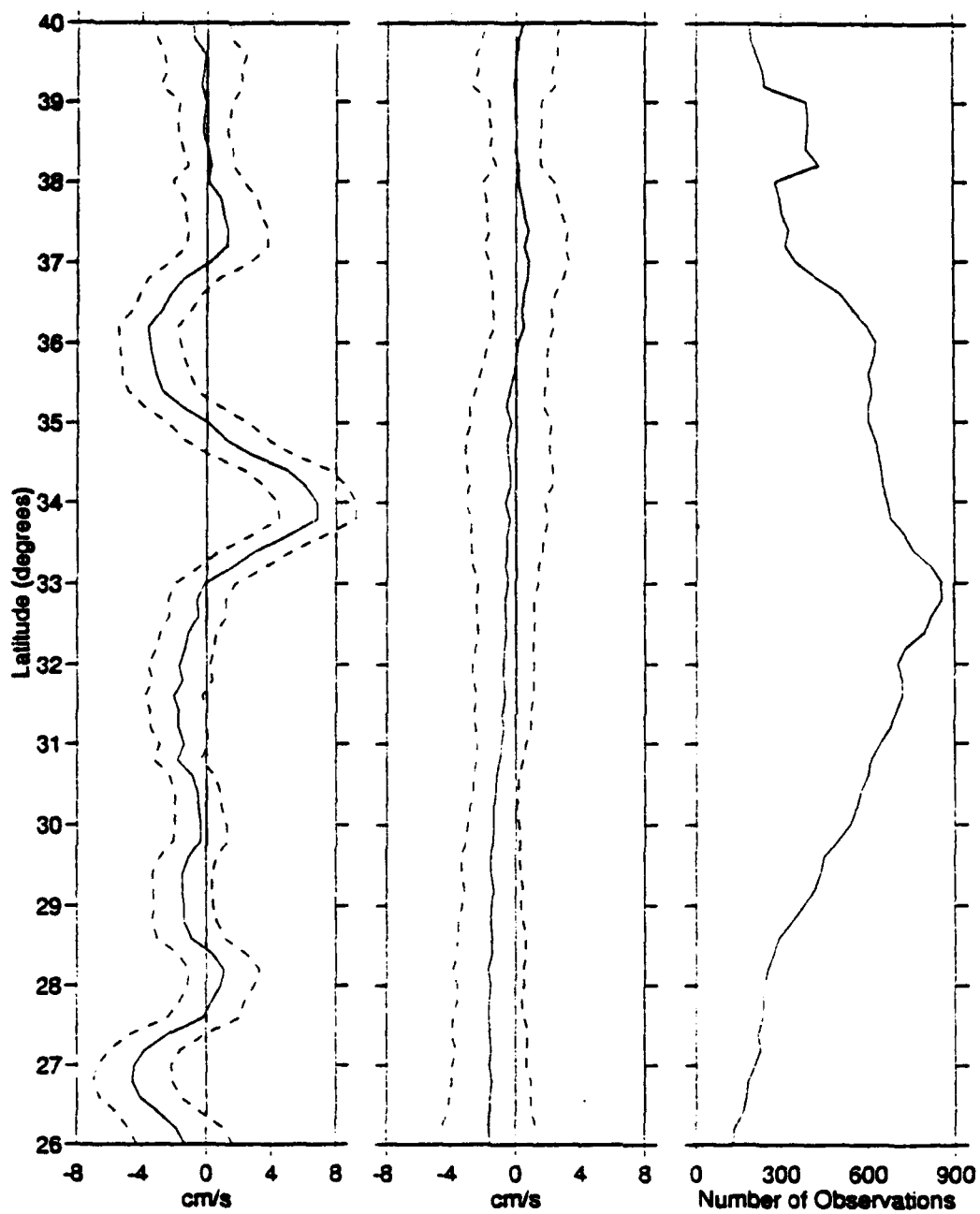


Figure 20. Zonal average of eastward (left) and northward (middle) velocity and their standard errors (dashed) with the number of 2-day-interpolated observations in 1 degree latitude bands (right).

#### IV. SINGLE PARTICLE LAGRANGIAN STATISTICS

The basic statistics presented in the previous section did not take explicit advantage of the water-following nature of the drifter observations. It is also possible to compile important velocity statistics based on the average behavior of an ensemble of drifters. In particular, measurements of the Lagrangian autocovariance provide indications of the time and length scales of particle motions. They also provide indications of the rapidity with which particles wander away from their initial positions (their dispersion rates and diffusivities) and direction in which particles rotate (clockwise or counterclockwise).

In order to compute the Lagrangian autocovariance and the other flow indicators that derive from it, continuous time series of drifter positions are required. The length of the time series must significantly exceed the integral time scale of the motions. For this data set, the continuous time series are provided by the 2-day-interpolated trajectories from individual drifters. The integral time scale will be shown to be less than 10 days. Hence, the minimum length the drifter trajectory is several times that value. In this study, trajectories less than 49 days in length were not used to compute Lagrangian autocorrelations.

Ensemble averages of Lagrangian statistics were performed for the entire suite of drifter trajectories. They were also performed for ensembles of drifters confined to the large regions in the South, North, and Frontal Zone and for ensembles of drifters confined to particular seasons as described for the basic statistics. There were some necessary differences, however, in the partitioning of drifter trajectories into regions or seasons between the Eulerian approach used for the basic statistics and the Lagrangian approach based on continuous trajectories. In order to obtain, at least, several trajectories in each ensemble, the physical boundaries of the regions were allowed to vary. In particular, the South region ensemble was formed from all drifter trajectories that spent at least 80% of their lifetime south of  $33^{\circ}$  N. The North region ensemble was formed from all drifter trajectories that spent at least 80% of their lifetime north of  $35^{\circ}$  N. These ensembles or



"families" of drifters therefore spent part of their lifetime within another region. The family of drifters chosen to describe the average statistics in the Frontal Zone actually overlapped even more with other regions. Because drifters with trajectories in the band between 33° N and 35° N tended to spend a large part of their lifetime outside that band, it was necessary to expand the Frontal Zone definition for the purposes of the Lagrangian statistics. For this study, the family of drifters chosen to represent the Frontal Zone were those drifters whose trajectories spent at least 75% of their lifetime between 33° N and 36° N. This gave significant overlap with the North family (Figure 6) but the flow characteristics of the Frontal Zone are different enough from those to the south and north that it stands out significantly in the Lagrangian statistics below.

Ensembles or families of drifter trajectories were also chosen to represent the seasons defined in TABLE I. This was done by picking out the portions of trajectories in each season and treating them like separate drifters as long as the duration of the trajectories exceeded 49 days.

## A. LAGRANGIAN AUTOCOVARIANCES

The Lagrangian autocovariance function is the averaged time-lagged covariance of velocity following a drifter trajectory. It is computed according to the following formula (Davis, 1983):

$$R_{ij}(\tau, T, x_o, t_o) \equiv \frac{1}{T} \int_{t_o}^{t_o+T} u_i'(t, x_o, t_o) u_j'(t + \tau, x_o, t_o) dt \quad \begin{cases} i = u, v \\ j = u, v \end{cases} \quad (2)$$

The right hand side of (2) can be also written as  $\langle u_i'(t, x_o, t_o) u_j'(t + \tau, x_o, t_o) \rangle_L$  to be consistent with some literature where  $\langle () \rangle_L$  is a Lagrangian average. Here  $u' = u - \bar{u}$  is the eastward velocity perturbation and  $v' = v - \bar{v}$  is the northward velocity perturbation about the mean over time  $t_o$  to  $t_o+T$ .

The velocity components  $u(t, x_o, t_o)$ ,  $v(t, x_o, t_o)$  in (1) refer to the velocity at time  $t$  of the drifter passing through  $x_o$  at the initial time  $t_o$ . If the velocity field is assumed to be

stationary and homogeneous, the dependence on the initial point vanishes and equation (2) simplifies to (Taylor, 1921; Poulain and Niiler, 1989; Paduan and Niiler, 1993):

$$R_{ij}(\tau, T) \equiv \frac{1}{T} \int_0^T u_i'(t) u_j'(t + \tau) dt \quad \begin{cases} i = u, v \\ j = u, v \end{cases} \quad (3)$$

The zero-lag autocovariances  $R_{uu}(0, T)$ ,  $R_{vv}(0, T)$  are simply the velocity variances in the east-west and north-south directions, respectively, for the time series of length  $T$ . For the purposes of ensemble averages over many drifters, the Lagrangian autocorrelation function is formed by normalizing the autocovariance by the variance before averaging.

The autocovariance (or autocorrelation) functions are expected to asymptote smoothly to zero in the presence of homogeneous and stationary turbulence. For the 2-day-interpolated velocity data in this study, mesoscale eddies provide the turbulent-like decay. The degree to which the functions fail to asymptote to zero provides a measure of the non-homogeneity of the velocity field.

The average time-lagged autocorrelation functions for eastward and northward velocity components are presented in Figure 21 for the ensemble of all drifters and for the families of drifters in the South, North, and Frontal Zone regions as defined above. The comparable functions for the seasonal drifter ensembles are presented in Figure 22. In all cases, the standard error of the mean autocorrelation function is presented for each velocity component at each time lag. These errors were computed assuming each drifter trajectory provided an independent autocorrelation function, i.e. the number of independent observations in (1),  $N^* = N$ , where  $N$  is the number of drifters in the ensemble.

The averaged autocorrelation functions are quite well behaved for all ensembles. The time scale for the decay of the functions is in the range of 5 to 10 days for all cases. (These values are quantified below.) There is not an obvious difference in the shapes of the functions for the different regions and seasons. The eastward and northward correlation functions are similar but the northward functions decay faster in all cases. The error bars show that each of the averages are quite well defined. These functions are the bases for the following computations of time scales, length scales, diffusivities, and polarization.

## 1. Integral Time Scales

The Lagrangian integral time scale provides a measure of the time over which a drifter remembers its path. An objective measure of this time scale is made for each drifter according to:

$$T_L = \frac{1}{R(0)} \int_0^{\infty} R(\tau) d\tau \quad (4)$$

In practice, the infinite limit of integration is replaced by a finite time,  $T_{max}$ , greater than the expected time scale but short enough to avoid including the oscillatory portion of the covariance function that may exist due to inhomogeneities. Calculations of  $T_L$  were made separately for east-west and north-south motions with  $T_{max} = 10$  days. The average  $T_L$  for each drifter ensemble was calculated by averaging  $T_L$  for each drifter in the ensemble. Standard errors for these averages were computed assuming each drifter provided an independent estimate of the time scale.

The average Lagrangian integral time scales for east-west and north-south drifter motions are presented in TABLE IV for each drifter ensemble. Standard errors of the means and the number of drifters in each ensemble are all presented in the table. The time scale estimates are quite significant in all cases. The average time scales determined using the 35 longest drifter trajectories are 6.4 days and 4.9 days for the east-west (zonal) and north-south (meridional) directions, respectively. Time scales are longer for east-west motions than for north-south motions in all ensembles. This is consistent with the observations of stronger eastward currents appearing in various latitude bands. Particles (drifters) move further distances in the east-west direction under the influence of an organized flow than they do in the north-south direction.

The longest time scales in TABLE IV are for the overall ensemble and for the South ensemble, although they are not statistically larger than the estimates for most of the remaining ensembles. It should be noted that the results obtained using all drifters are not the algebraic average of either the three regional ensembles or the four seasonal ensembles. This is because some trajectories are not present in any of the regional ensembles (and

TABLE IV. MEAN AND STANDARD ERROR (IN PARENTHESIS) OF THE ENSEMBLE-AVERAGE TIME SCALE BASED ON DRIFTERS POSITION.

	TIME SCALES (days)		
ENSEMBLE	ZONAL	MERIDIONAL	N
<i>ALL DATA</i>	6.39 (0.67)	4.94 (0.51)	35
<i>FALL</i>	4.77 (0.75)	4.14 (0.81)	42
<i>WINTER</i>	4.92 (0.76)	4.53 (0.79)	48
<i>SPRING</i>	4.74 (0.96)	3.65 (0.86)	47
<i>SUMMER</i>	4.51 (0.99)	3.73 (0.77)	38
<i>NORTH</i>	5.31 (1.51)	4.89 (1.08)	10
<i>FRONT-ZONE</i>	5.76 (1.14)	4.92 (1.29)	10
<i>SOUTH</i>	6.58 (1.07)	5.41 (1.01)	7

some are present in more than one) and, in the case of the seasonal ensembles, portions of the drifter trajectories within the seasonal boundaries are considered as separate trajectories.

## 2. Integral Length Scales

The integral time scales given above have an associated integral length scale,  $L$ , when combined with a typical velocity scale. If we assume a random walk,  $L$  is related to the distance over which the particle remembers its path (Krauss and Böning, 1987). It is given by

$$L = \sqrt{\sigma^2} \cdot T_L \quad (5)$$

where  $\sigma^2$  is the velocity variance.

The average Lagrangian integral length scales for east-west and north-south drifter motions are presented in TABLE V for each drifter ensemble. Standard errors of the

means and the number of drifters in each ensemble are also presented in the table. The average length scales determined using the 35 longest drifter trajectories are 57 km and 39 km in the east-west and north-south directions, respectively. The length scales are consistently larger in the east-west direction than in the north-south direction. This is expected given the longer east-west time scales but it is possible that changes in velocity variances are independent of changes in time scales. This is the case for the length scales computed for the Frontal Zone ensemble. Because the variances are much larger for that region (TABLE II), the length scales are larger than for the other ensembles.

## B. DIFFUSIVITY

A measure of the rate of spreading of a particle from its initial position is provided by the diffusivity, which gives the rate of change of the root mean square (rms) particle position relative to the mean trajectory of the particle. Under the conditions of stationarity

TABLE V. MEAN AND STANDARD DEVIATION (IN PARENTESIS) OF THE ENSEMBLE-AVERAGE LENGTH SCALE BASED ON DRIFTERS POSITION.

	LENGTH SCALES (Km.)		
ENSEMBLE	ZONAL	MERIDIONAL	N
<i>ALL DATA</i>	56.5 (8.41)	39.3 (5.80)	35
<i>FALL</i>	39.0 (9.71)	29.1 (6.61)	42
<i>WINTER</i>	39.4 (8.59)	34.7 (6.72)	48
<i>SPRING</i>	42.8 (10.4)	25.1 (6.70)	47
<i>SUMMER</i>	35.3 (10.4)	26.8 (7.30)	38
<i>NORTH</i>	38.2 (11.8)	35.0 (11.4)	10
<i>FRONT-ZONE</i>	54.4 (14.1)	43.7 (16.5)	10
<i>SOUTH</i>	48.7 (11.7)	37.2 (9.50)	7

and homogeneity, the diffusivity is related to the autocovariance according to the following formula (Taylor, 1921):

$$K_{ii}(t) = \int_0^t R_{ii}(\tau) d\tau \quad \begin{cases} i = u, v \\ j = u, v \end{cases} \quad (6)$$

Note that, computationally, the diffusivity formula in (6) is similar to that for the integral time scales in (4).  $K_{uu}$  and  $K_{vv}$  are computed from the autocovariance functions with normalization. Like the autocovariance functions, the diffusivities are expected to asymptote to a constant value, called the saturation value, within a few integral time scales.

The average diffusivity functions for eastward and northward velocity components are presented in Figure 23 for the ensemble of all drifters and for the families of drifters in the South, North, and Frontal Zone regions as defined above. The comparable functions for the seasonal drifter ensembles are presented in Figure 24. The functions do peak for times equal to 1 to 2 integral time scales. The expected asymptotic behavior is modified by weeks-long oscillations in the diffusivity functions, particularly for the seasonal ensembles. This reflects inhomogeneities in the flow field. Negative slopes of diffusivity functions imply negative diffusion, which is not expected. Instead, the model of mesoscale eddies acting like random turbulence on one time scale, namely the integral time scale, is not valid. Longer period organized motions exist in addition to those of the dominant eddies.

The ensemble-averaged diffusivity functions are all significantly greater than zero, particularly for the over all ensemble. In all cases, the east-west diffusivities are greater than the north-south diffusivities. The effective diffusivity for a given region is usually given by the saturation value achieved after some short time. In order to approximate that value, the diffusivity levels at time  $t = T_{max}$  were chosen where  $T_{max} = 10$  days.

The average east-west and north-south diffusivities and their standard errors are presented in TABLE VI for each ensemble. The average diffusivities determined using the 35 longest drifter trajectories are  $6.2 \times 10^7$  cm<sup>2</sup>/sec and  $3.8 \times 10^7$  cm<sup>2</sup>/sec for the east-west and north-south directions, respectively. The east-west diffusivities are 1.5 to 2 times larger than the north-south diffusivities in all cases. In the regional ensembles, the Frontal

Zone diffusivities are significantly larger than those calculated for the South or North regions. This is consistent with the higher energy levels in that region. The seasonal ensembles show no particular pattern. The value of east-west diffusivity in the Spring ensemble is large compared with the other time periods.

TABLE VI. AVERAGE ZONAL ( $K_{UU}$ ) AND MERIDIONAL ( $K_{VV}$ ) DIFFUSIVITY AND THEIR STANDARD ERROR (S.E.) FOR ENTIRE DATA SET AND BY REGION AND SEASON.

DIFFUSIVITY ( $10^7 \text{ cm}^2/\text{s}$ )		
	$K_{uu}$ (S.E.)	$K_{vv}$ (S.E.)
<b>ALL AREA</b>	6.2 (1.3)	3.8 (0.8)
<b>FALL</b>	4.3 (1.6)	2.8 (0.8)
<b>WINTER</b>	4.3 (1.4)	3.3 (0.8)
<b>SPRING</b>	5.1 (1.8)	2.2 (0.7)
<b>SUMMER</b>	3.7 (1.5)	2.6 (1.2)
<b>NORTH</b>	3.3 (1.3)	3.1 (1.4)
<b>FRONT-ZONE</b>	6.1 (2.2)	4.8 (3.0)
<b>SOUTH</b>	4.4 (1.6)	3.0 (1.0)

The average diffusivities are expected to scale with the kinetic energy of the flow field (Krauss and Böning, 1987; Poulain and Niiler, 1989; Paduan and Niiler, 1993). The results from the ensembles in this study can be compared with each other and with previous drifter studies. The comparisons are given in TABLE II and TABLE III for the EKE and—in the case of the overall ensemble—for the diffusivity. A plot of diffusivity versus EKE is presented in Figure 25 for the results of this study and previous drifter studies. In this case, the diffusivity is the average of  $K_{uu}$  and  $K_{vv}$ . In general, diffusivity is larger for larger EKE. The value from the CTZ Experiment in the California Current (Brink et al., 1991) is anomalous. The EKE is high relative to the diffusivity. This is explained by the

nature of the drifter measurements in the CTZ Experiment. The drifters were placed into known upwelling filaments off the California coast, which represents a biased sample of the flow field (Paduan and Niiler, 1990; Brink et al., 1991). The trajectories in these features do not follow the classical dispersion notion of random turbulence. Without the CTZ value, the best-fit linear line through the averages from the other four experiments gives the following result:

$$K = -7.02 \times 10^6 + 4.76 \times 10^5 \text{EKE} \quad (7)$$

where the units of  $K$  are  $\text{cm}^2/\text{sec}$  and the units of EKE are  $\text{cm}^2/\text{sec}^2$ . The best-fit line is included in Figure 25 for reference. The model accounts for 82% of the variance in the four data points. In physical terms, the model suggests an integral time scale of 5.5 days as the constant of proportionality.

Alternatively, diffusivity could be fit to the rms velocity, which suggests an integral length scale as the constant of proportionality. The best-fit line for this alternate model is:

$$K = -3.74 \times 10^7 + 7.82 \times 10^6 (\text{rms velocity}) \quad (8)$$

where the units of rms velocity are in  $\text{cm}/\text{sec}$ . This model is equally as good as the model using EKE (it explains 80% of the variance in the four data point). It implies a universal integral length scale of 78 km. At this stage, it is not possible to distinguish between the two models (7) and (8) for diffusivity. However, it is clear that diffusivity does scale with energetics of the velocity field, which could be a useful result for numerical modelers working with sufficient resolution to simulate the actual effects of mesoscale eddies.

## 1. Array Bias

The average north-south diffusivity in the SUBDUCTION region,  $K_{vv} = 3.8 \times 10^7 \text{ cm}^2/\text{sec}$ , can be used to investigate the apparent divergence of the zonally-averaged northward velocity (Figure 20). Drifter-derived velocity averages may be biased by non-uniform concentrations in the presence of turbulent diffusion. The error is known as the array bias and is given by (Davis, 1993):



$$-K_w \frac{\partial}{\partial y} (\ln C) \quad (9)$$

where  $C$  is a measure of the particle (drifter) concentration. In order to estimate the size of this error in the SUBDUCTION drifter data set, a measure of the two-dimensional concentration is required. This was estimated by making a simple linear approximation to the number of 2-day-interpolated observations as a function of latitude shown in Figure 20. The number of 2-day-interpolated observations was approximated as 800 at the latitude of 33° N and was assumed to decrease linearly to 400 at locations 400 Km north and south of that latitude. A schematic representation of this approximation is given in Figure 26.

In order to convert the approximation of the number of observations into a concentration estimate, the maximum number of independent velocity observations per latitude band was computed for the duration of the measurement (2 years). Again, this is represented schematically in Figure 26. Typical time and length scales of 5 days and 40 Km, respectively, were used to compute the maximum number of independent velocity estimates within a 1 degree latitude band:

$$N^{Max} = \frac{\left[ (100\text{km})(2000\text{km})(2\text{yr}) \left( \frac{365\text{day}}{\text{yr}} \right) \right]}{(40\text{km})^2 (5\text{day})} = 18250$$

The maximum concentration at 33° N is, therefore, estimated as:

$$C^{Max} = \frac{800}{18250} = 0.0438$$

The concentration is half that value 400 Km to the north or south of 33° N.

With these crude estimates of concentration, the error in the zonally-averaged northward velocity due to the array bias can be estimated. The magnitude of the error according to (9) is estimated by:

$$\begin{aligned}
|\text{Array Bias}| &= K_w \left| \frac{\partial}{\partial y} (\ln C) \right| \\
&= \left( 3.8 \times 10^7 \frac{\text{cm}^2}{\text{sec}} \right) \left| \frac{\ln(0.0438) - \ln\left(\frac{0.0438}{2}\right)}{4 \times 10^7 \text{cm}} \right| \\
&= 0.7 \frac{\text{cm}}{\text{sec}}
\end{aligned}$$

Given the slopes of the concentration north and south of the central latitude, the array bias is estimated to have produced an erroneous northward current 0.7 cm/sec in the north and -0.7 cm/sec in the south. This represents a large-scale divergence of the surface velocities of the same order as was observed in the zonally-averaged northward current (Figure 20). Hence, the data set used in this study was sufficiently biased by the distribution of the observations to mask the expected large-scale convergence.

### C. POLARIZATION

The drifter trajectories in this study often exhibit a looping or circular behavior, which is attributed to eddies. The direction of rotation of the trajectories can be determined from combinations of the covariance functions between east-west and north-south currents. This direction of rotation is of interest in the characterization of the eddy field. The cumulative (or average) rotation for a given drifter is given by the following integral of the covariance functions (Poulain and Niiler, 1989):

$$J(t) = \int_0^t (R_{uv}(\tau) - R_{vu}(\tau)) d\tau \quad (1)$$

$J$  is referred to as the polarization in this study. It is referred to as the integral of the polarization by some authors (Poulain and Niiler, 1989; Paduan and Niiler, 1993).

If the function  $J$  is positive, the drifter trajectory is more often rotating cyclonically (counterclockwise). If  $J$  is negative, the trajectory is more often rotating anticyclonically. The average polarization is presented in Figure 27 for the ensemble of all drifters and for

the families of drifters in the South, North, and Frontal Zone regions as defined above. The comparable functions for the seasonal drifter ensembles are presented in Figure 28. Because these functions depend on the Lagrangian autocovariance functions and the assumptions of homogeneity and stationarity, values for times much greater than the integral time scales should be ignored. In keeping with the integration times used above for the integral time scales and diffusivities, only the polarization for lag times up to 10 days is considered.

Most of the polarization functions in Figure 27 and Figure 28 show no preference for cyclonic or anticyclonic rotation that exceed the error bars. The average for the overall, fall, and Frontal Zone ensembles show significant preferences for anticyclonic rotation with the largest values for the Frontal Zone ensemble.

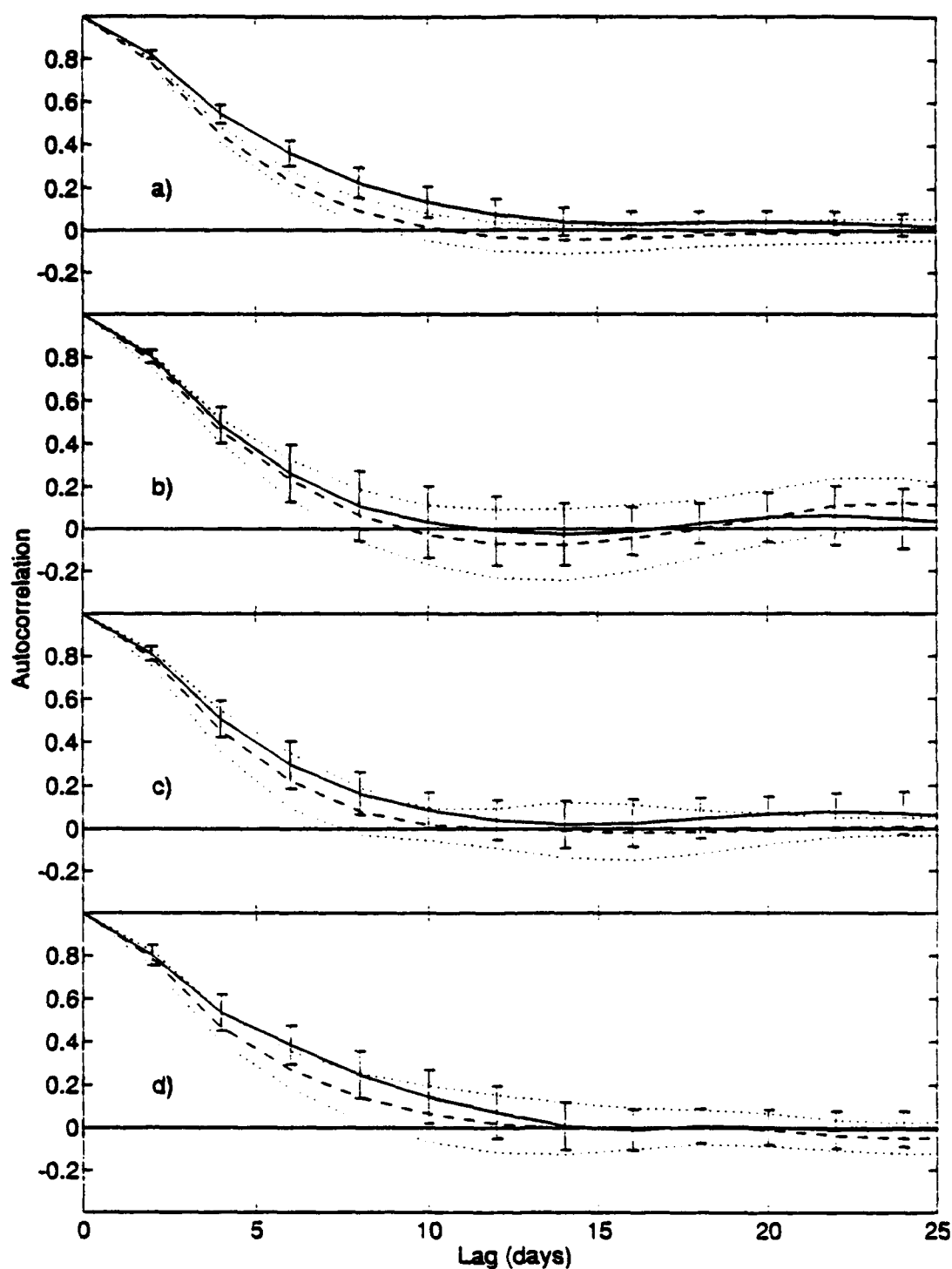


Figure 21. Ensemble-averaged autocorrelation functions and their standard errors—assuming each drifter provided an independent estimate—for east-west (solid; error bars) and north-south (dashed; error envelopes) velocity components for the ensemble of all drifters (a), the North ensemble (b), the Frontal Zone ensemble (c), and the South ensemble (d).

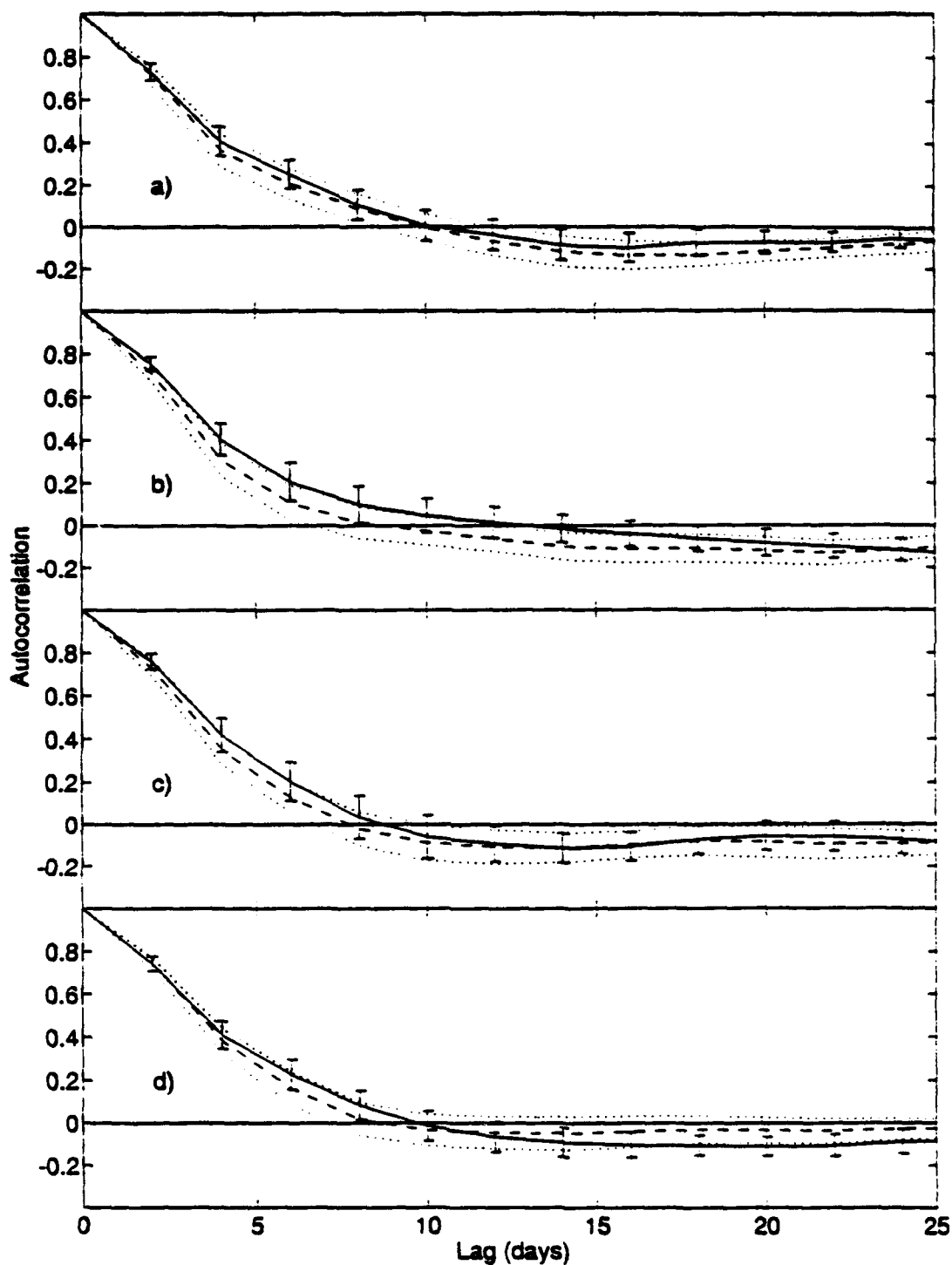


Figure 22. Ensemble-averaged autocorrelation functions and their standard errors—assuming each drifter provided an independent estimate—for east-west (solid; error bars) and north-south (dashed; error envelopes) velocity components for the Winter ensemble (a), the Spring ensemble (b), the Summer ensemble (c), and the Fall ensemble (d).

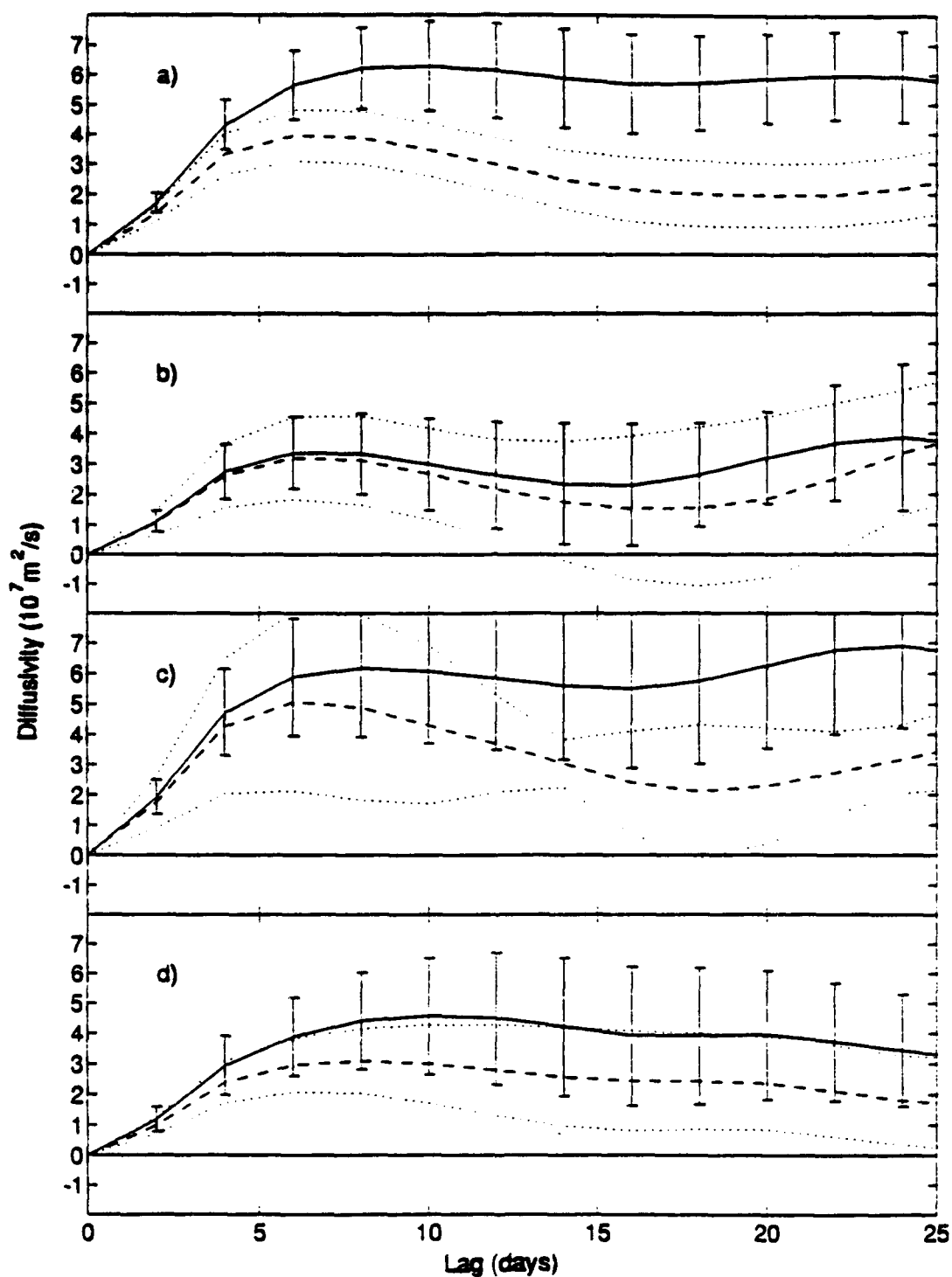


Figure 23. Ensemble-averaged diffusivities and their standard errors—assuming each drifter provided an independent estimate—for east-west (solid; error bars) and north-south (dashed; error envelopes) velocity components for the ensemble of all drifters (a), the North ensemble (b), the Frontal Zone ensemble (c), and the South ensemble (d).

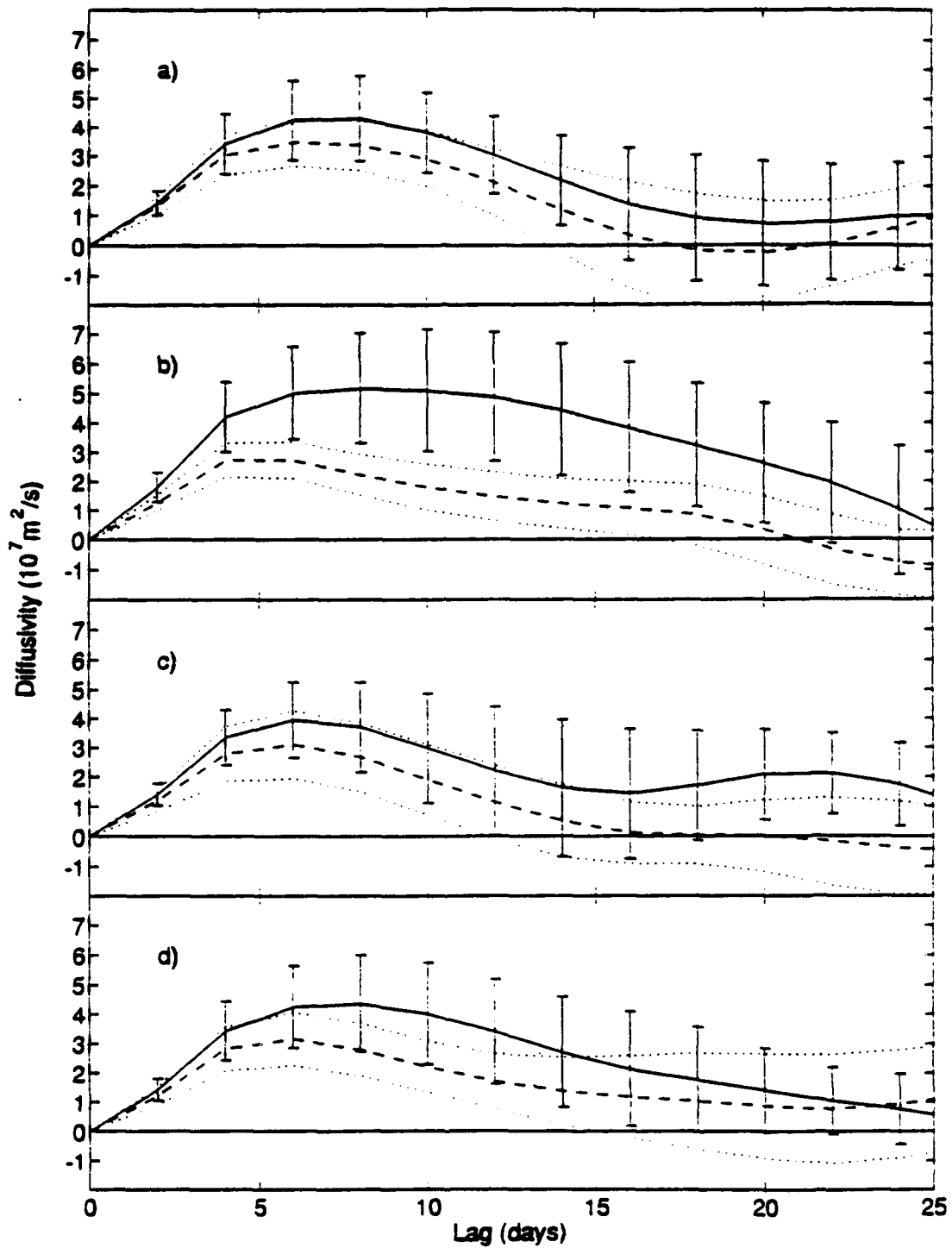


Figure 24. Ensemble-averaged diffusivities and their standard errors—assuming each drifter provided an independent estimate—for east-west (solid; error bars) and north-south (dashed; error envelopes) velocity components for the Winter ensemble (a), the Spring ensemble (b), the Summer ensemble (c), and the Fall ensemble (d).

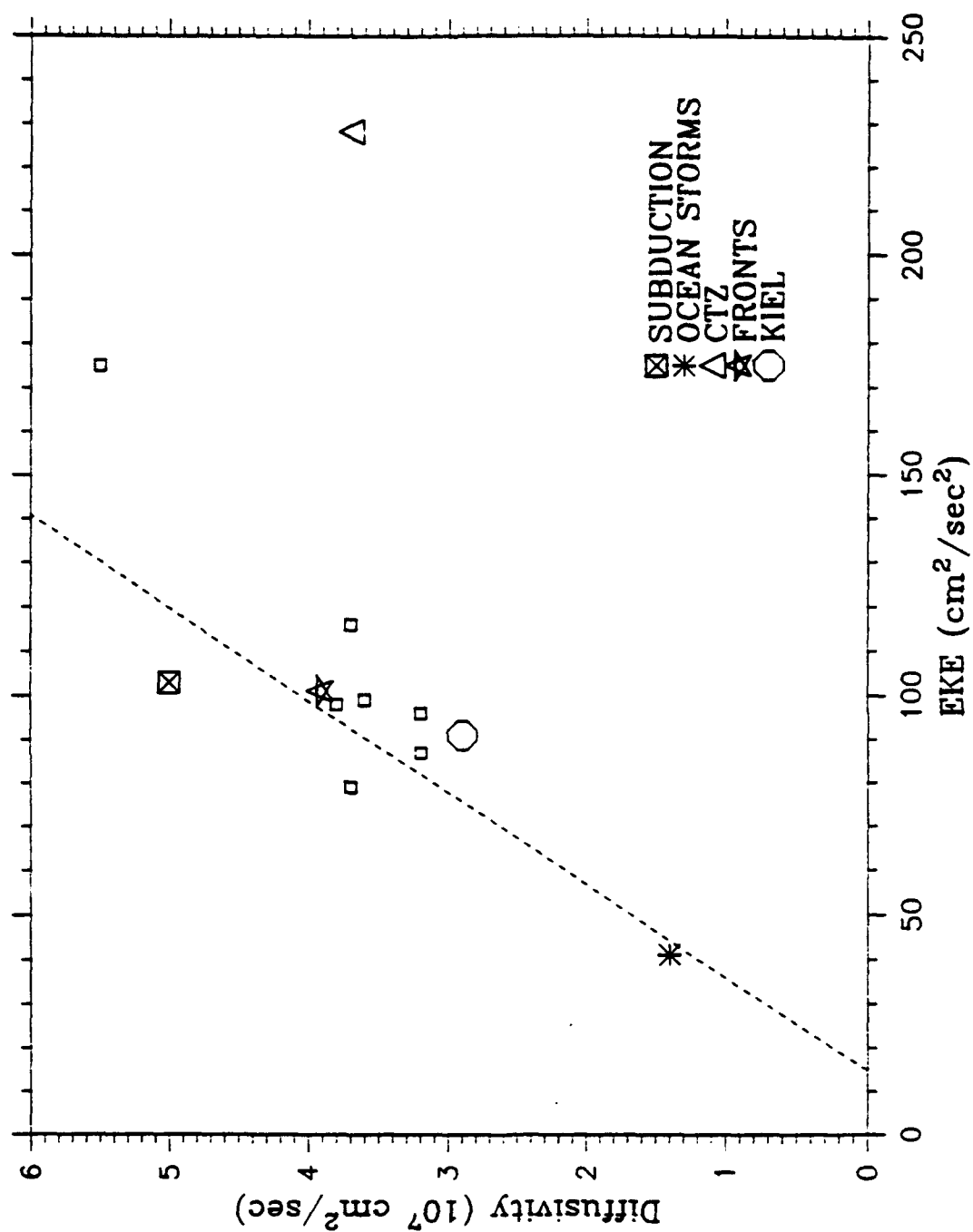


Figure 25. Average diffusivity versus Eddy Kinetic Energy for the ensembles used in this study (small squares) and the overall results of this study and four previous drifter studies (see legend).



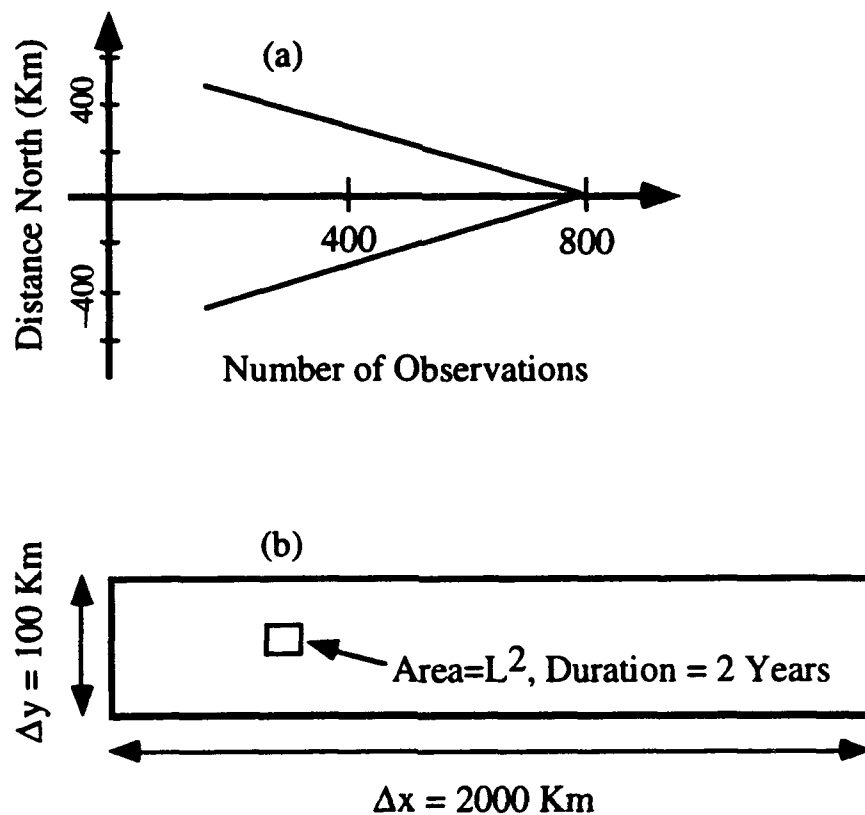


Figure 26. Schematic representations of the distribution of 2-day-interpolated observations relative to the central latitude of  $33^\circ \text{ N}$  (a) and the maximum number of independent observations in a zonal average over the two-year period of the measurements (b).

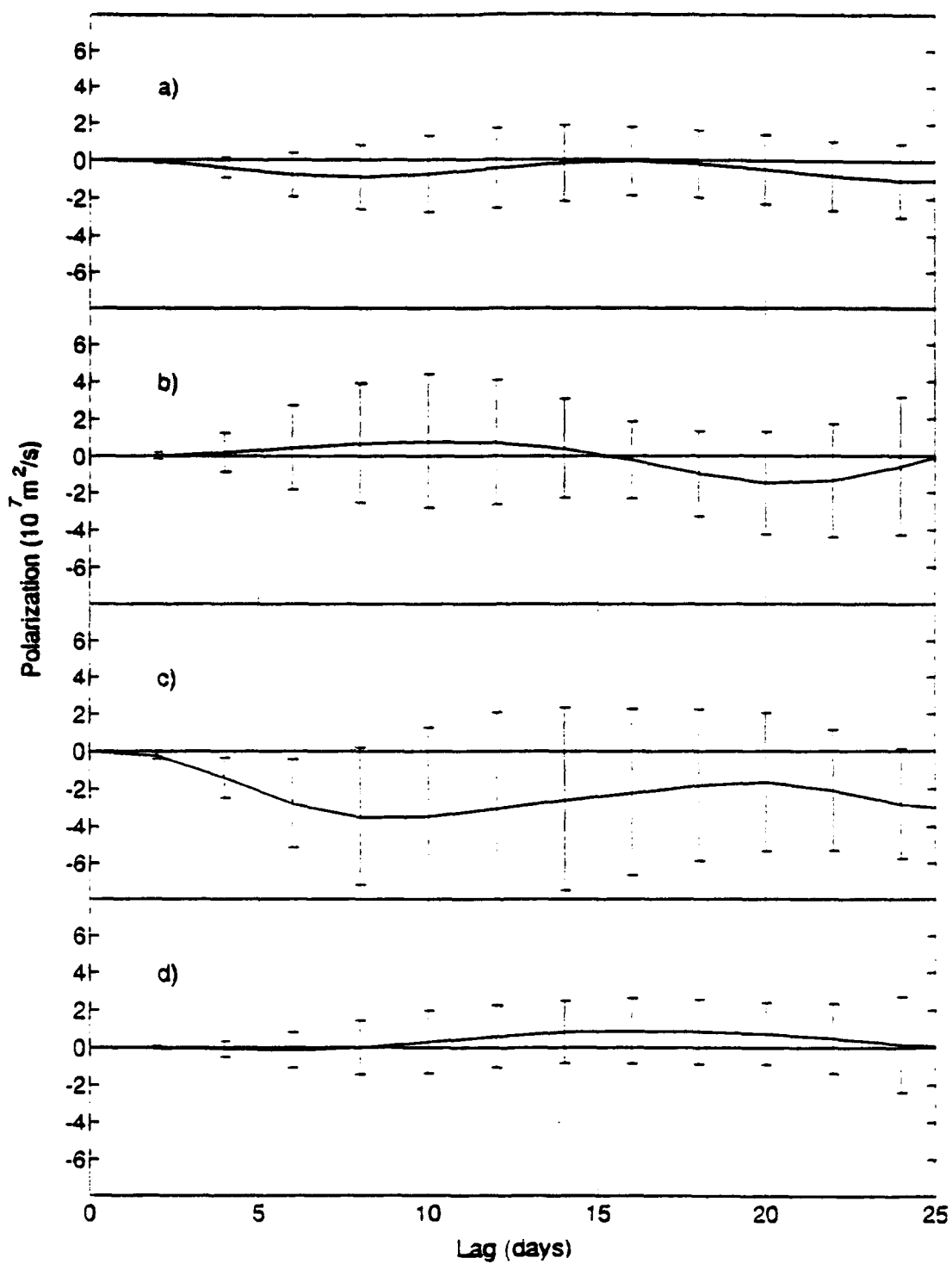


Figure 27. Ensemble-averaged polarization functions and their standard errors—assuming each drifter provided an independent estimate—for the ensemble of all drifters (a), the North ensemble (b), the Frontal Zone ensemble (c), and the South ensemble (d).

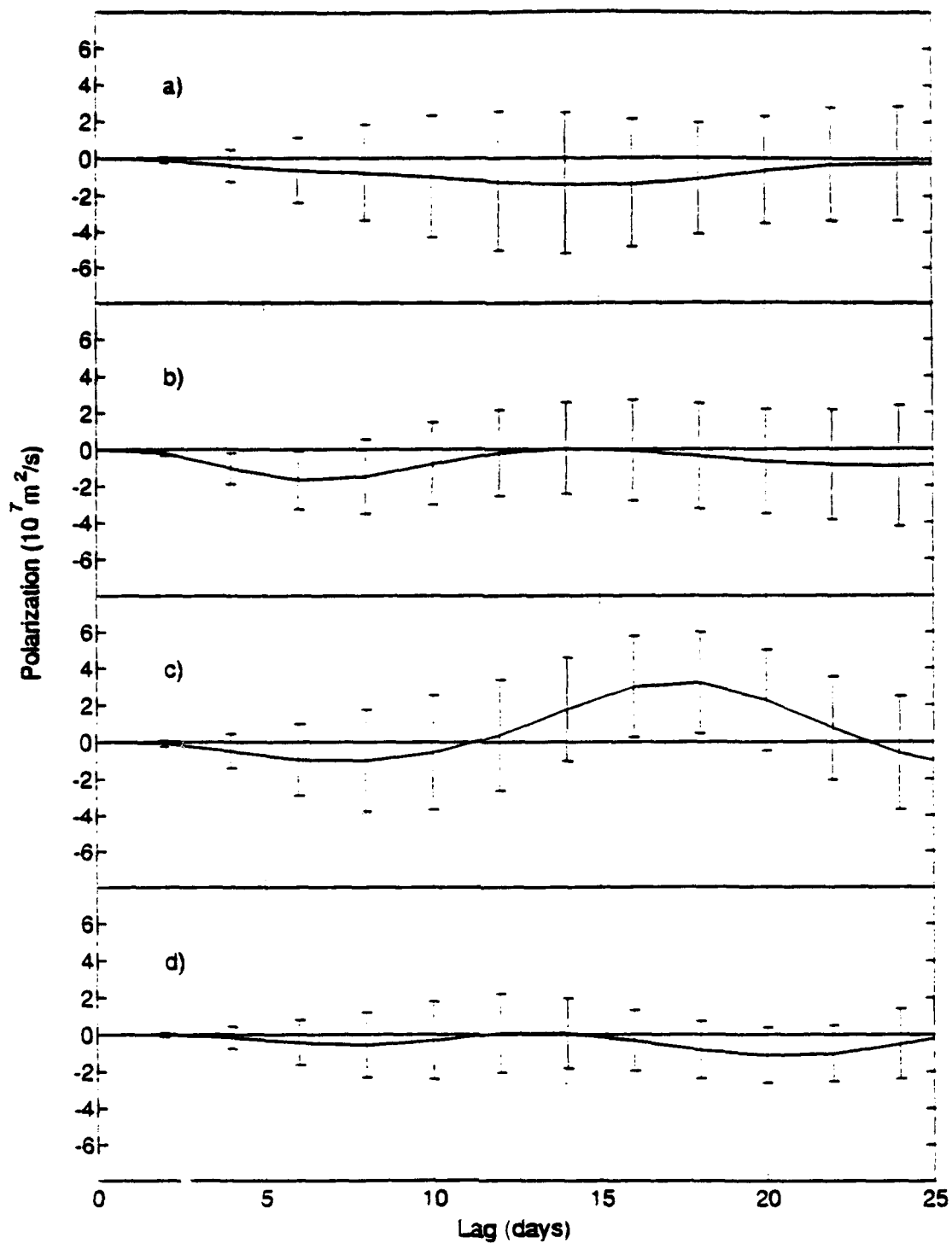


Figure 28. Ensemble-averaged polarization functions and their standard errors—assuming each drifter provided an independent estimate—for the Winter ensemble (a), the Spring ensemble (b), the Summer ensemble (c), and the Fall ensemble (d).

## **V. EDDY SURVEY**

Mesoscale eddies have played an important role throughout the analysis of this data set. It is of interest to characterize the eddies in the drifter trajectories both to understand them as a source of noise to the observation of mean currents and in their own right as agents of transport and mixing of water properties. In the case of data sets with large numbers of trajectories such as the one analyzed in this study, it is difficult to search for and describe individual eddies. In this section a simple mathematical method for investigating drifter trajectories is proposed in the hope that it may be useful in objectively selecting looping portions of the trajectories. No conclusions are drawn about the method at this time.

### **A. SUBJECTIVE METHOD**

The traditional method of finding loops or eddies in drifter trajectories is to study each trajectory and subjectively select those portions associated with eddy-like features. As an example, Figure 29 shows a composite of the eddy-like portions of the trajectories used in this study. Most of the eddy activity selected in this way is in the latitude range of the Frontal Zone.

### **B. OBJECTIVE METHOD**

An automated method for selecting looping portions of drifter trajectories would save time, particularly for large data sets. It would also have the advantage of removing subjectivity from the process. Such a method was tested with the data set used in this study. The method involved computing the radius of curvature of the trajectory as a function of time along the trajectory. This was done using three consecutive positions, which is the minimum possible number. The position data was converted into distances in kilometers east and north of the average position. Then the best-fit circle was subscribed

within the points and the radius of the circle was assigned to the time of the center point. The position data was then stepped ahead one point and the calculation repeated.

The histogram of all radius of curvature estimates for the entire data set is shown in Figure 30. The values of the histogram were normalized by the value of the maximum bin. The total number of 2-day observations was 7028. For this data set, the most common radii were in the range 8–20 Km with a uniform decrease in abundance above 16 Km. Radius histograms were also computed for all observations by season. The results are shown in Figure 31 for normalized histograms. In general, the seasonal histograms are quite similar to the overall histogram and to each other. There is a difference between the Spring and Fall histograms, however. In spring there were fewer small radii but more large radii. The summer and winter histograms are similar across the range of radii.

Given the radius of curvature assigned to each data point, it is possible to pick out drifter locations as a function of the curvature of the trajectory. As an example, Figure 32 shows all drifter locations with radii of curvature in the range 30–40 Km. In some cases, it is possible to identify continuous drifter trajectories and some eddy-like features in the figure. In general, however, this objective map does not identify the eddies selected subjectively and shown in Figure 29.

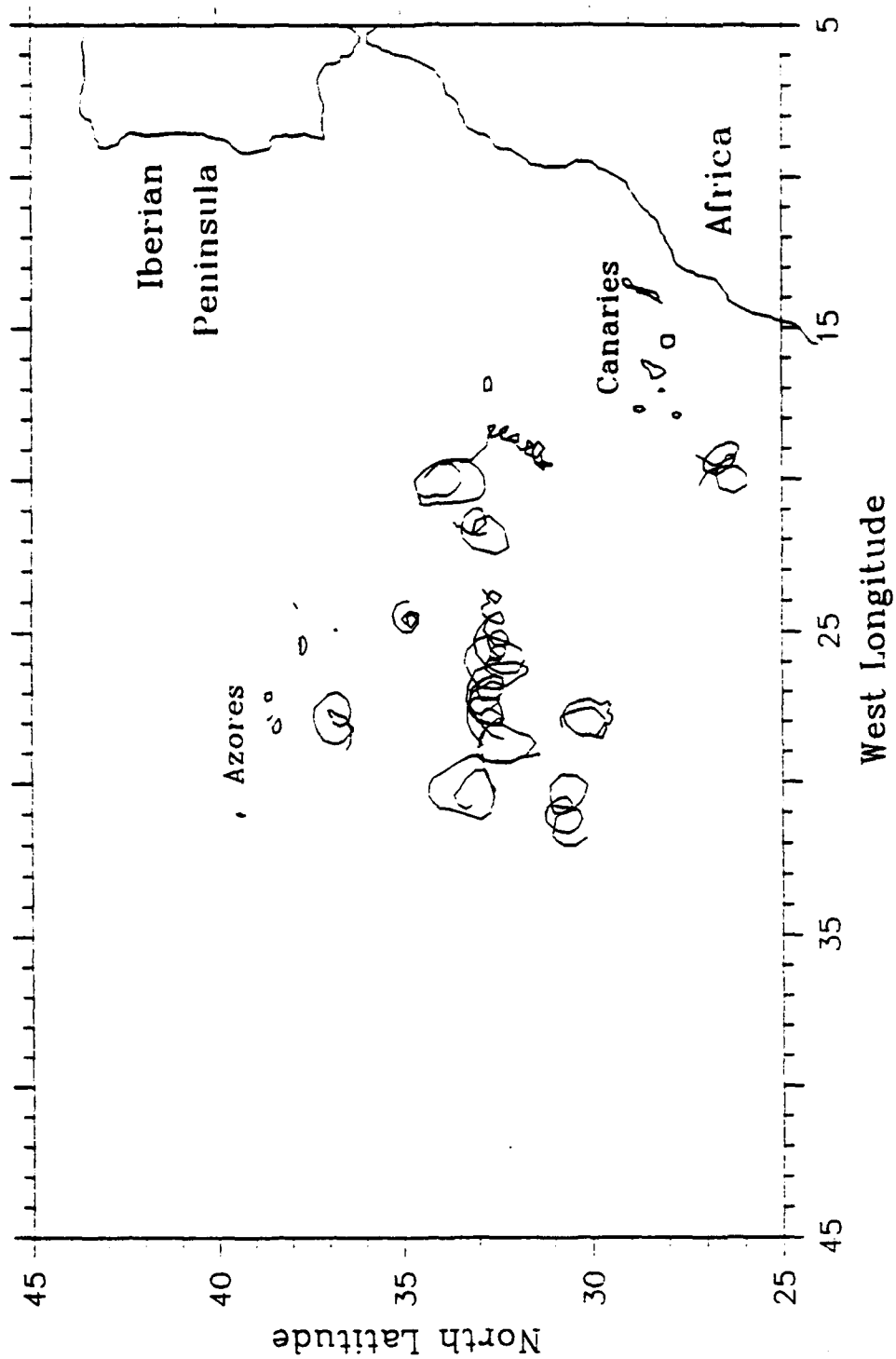


Figure 29. Portions of drifter trajectories belonging to eddies as determined from a subjective survey.

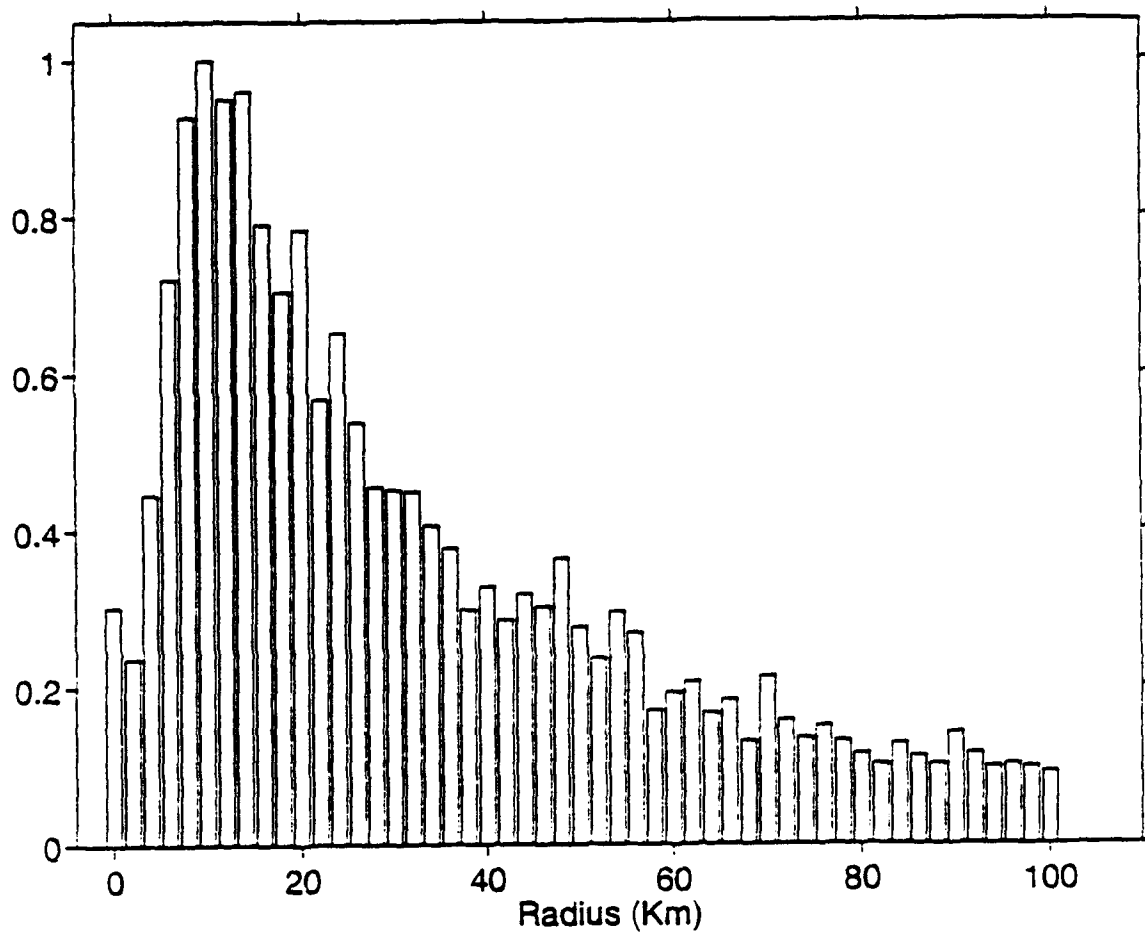


Figure 30. Normalized histogram of the radius of curvature for all observations. The total number of 2-day observations is 7028.

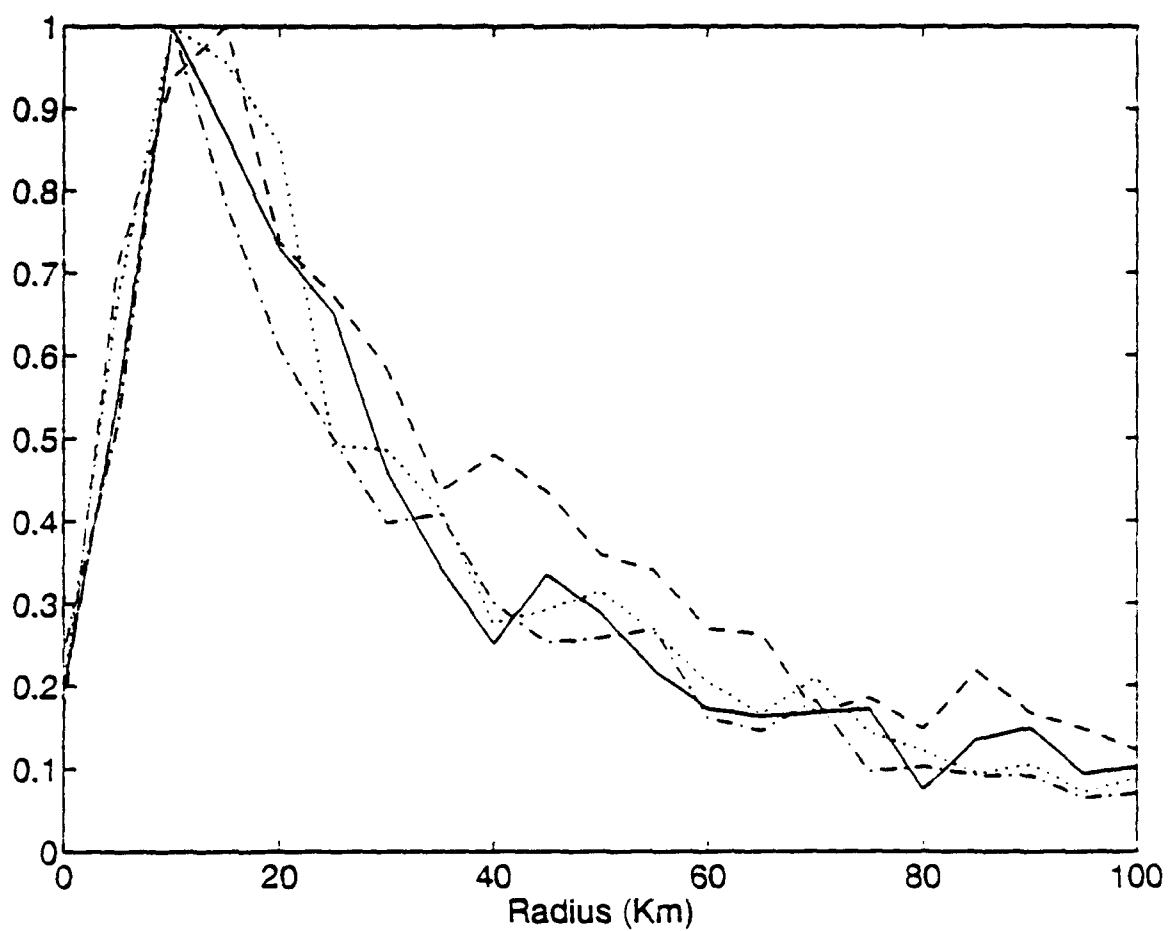


Figure 31. Normalized histogram of the radius of curvature by season for the winter (solid, 1954 points), spring (dashed, 1760 points), summer (dash-dot, 1569 points), and fall (dotted, 1745 points) periods.



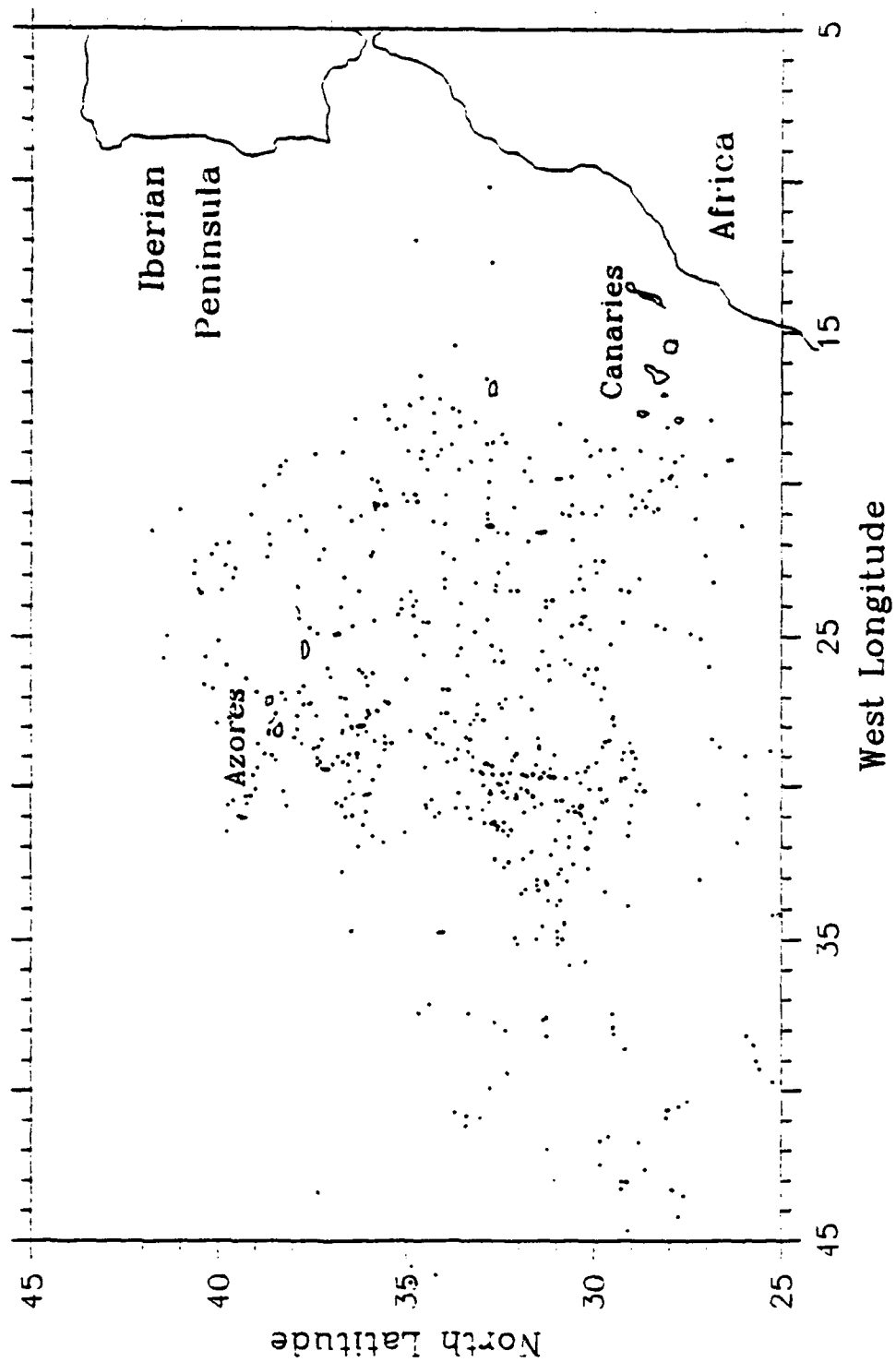


Figure 32. Drifter locations with radii of curvature in the range 30–40 Km.

## VI. CONCLUSIONS AND RECOMMENDATIONS

### A. CONCLUSIONS

Krauss and Käse (1984) observed as a last recommendation:

The main problem in defining eddy kinetic energy seems to be the separation of the mean current from the eddies. A much larger data set is needed in order to improve considerably the significance of the present result. This especially holds if one tries to obtain information about the seasonal variability.

This study has attempted to improve considerably the results of Krauss and Käse (1984) and others by analyzing a large set of surface drifter data from the SUBDUCTION region of the northeast Atlantic Ocean. Over 14,000 drifter days from 36 drifters over a two-year period were available. The problems raised by Krauss and Käse are still present, however, even in this large data set. The two-year mean velocity components were very small (less than 1.5 cm/sec) except in the region of the Azores Front where mean eastward currents were 3.9 cm/sec. The mean Eddy Kinetic Energy (EKE) value for the entire data set was  $103 \text{ cm}^2/\text{sec}^2$  but the value in the frontal zone was  $174 \text{ cm}^2/\text{sec}^2$ .

One of major goals of the experiment was to obtain enough observations to measure the surface convergence, particularly in the north-south direction. Even with the number of observations available in this study, the eddy currents are too strong relative to the mean currents to obtain statistically-significant mean currents as a function of latitude. It was also shown that the distribution of observations—which was concentrated around the central latitude of the study—may have led to erroneous currents on the order of the mean currents observed. This is due to the array bias where a non-uniform concentration of particles tend to diffuse away from regions of high concentration in the presence of a random turbulence field, which is unrelated to an actual mean current.

Classical Lagrangian single-particle statistics were computed on the whole data set and over ensembles of drifters separated by north-south regions and by time of year. In

general no seasonal patterns were found, although this may be due to the fact that no separation was made for both time of year and geographical location. Therefore, seasonal ensembles included data from all geographical locations. Significant differences were found for different regions. In particular, the area around the Azores front was found to have higher energy levels, length scales, and diffusivities.

The average integral time scales were  $4.9 \pm 0.5$  days and  $6.4 \pm 0.7$  days for east-west and north-south motions, respectively, where the error bars are the standard error of the mean assuming each drifter provided an independent estimate of the Lagrangian autocovariance function. The average integral length scales were  $56.5 \pm 8.4$  Km and  $39.3 \pm 5.8$  Km in the east-west and north-south directions, respectively. The average diffusivities were  $6.2 \pm 1.3 \times 10^7$  cm<sup>2</sup>/sec and  $3.8 \pm 0.8 \times 10^7$  cm<sup>2</sup>/sec for the same directions. In all cases, values were larger in the east-west directions implying longer time scales and larger length scales and diffusivities for that direction. This is consistent with the stronger zonal currents in the area. The direction or rotation of the trajectories, the polarization, showed no preference for cyclonic or anticyclonic rotation for most ensembles. There was significant preference for anticyclonic rotation in the region of the Azores Front, however.

The diffusivities and EKE levels found in this region were compared with previous drifter studies in the same area and in other areas. The results are consistent with the earlier studies. A plot of diffusivity versus EKE using average results from this and previous studies shows a good correlation confirming that diffusivity does scale with the energy level.

An objective method for selecting looping portions of drifter trajectories was presented based on the radius of curvature of the trajectory. This is an easily computed description of the particle paths that may be used to isolate portions of the path that are more or less eddy-like. For the observations in this study, the most common radius of curvature was around 16 Km but the most common eddies had radii of 30–50 Km.

## **B. RECOMMENDATIONS**

The primary recommendation for proceeding from this point is to obtain more data in order to improve the statistical reliability of the averages performed. At the end of the data period used in this study, there were still 24 drifters operating in the SUBDUCTION area. Another 25 drifters remain to be deployed as part of the SUBDUCTION Experiment. In addition, a French-Government-sponsored air-sea interaction experiment, called SEMAPHORE, is planned for this area and will include another 25 surface drifters similar to the ones used in this study. At the end of the lifetime of all drifters in the region, the available data set should be more than double the size of the one available in this study, assuming the instruments continue to function as well as they did in this phase of the experiment.

The selection of drifter ensembles for the Lagrangian statistics presented in Section IV used overlapping regions in the vicinity of the Frontal Zone in order to obtain enough drifters for each ensemble. This problem could be alleviated if psuedo trajectories were formed every integral time step and the records truncated to fixed lengths equal to several integral time steps in the manner of Poulain and Niiler (1989). This set of psuedo trajectories would be both larger and more evenly distributed than the original data set.

Finally, any calculation of mean currents from drifter data in the presence of a strong eddy field must be careful to account for array biases. In the case of the present data set, the concentration of deployments along latitude lines led to a very non-uniform concentration of particles. The strong diffusivities in the area led to significant errors in the mean currents when combined with this uneven distribution in the manner described by Davis (1993). As more data becomes available, this problem may dissappear, or it may be possible to subsample the data set to obtain more uniform coverage. These results show that care should be taken in designing a deployment scheme for drifters, particularly if the goal is the obtain a measure of the mean currents in a region of high eddy activity.

## REFERENCES

- Brink, K.H., R.C. Beardsley, P.P. Niiler, M. Abbott, A. Huyer, S. Ramp, T. Stanton, and D. Stuart, 1991: Statistical properties of near-surface flow in the California Coastal Transition Zone. *J. Geophys. Res.*, **96**, 14693-14706.
- Davis, R.E., 1983: Oceanic property transport, Lagrangian particle statistics, and their prediction. *J. Marine Res.*, **41**, 163-194.
- Davis, R.E., 1993: Observing the general circulation with floats. *Deep-Sea Res.*, **38**, Suppl 1, S531-S571.
- Davis, R.E., R.A. deSzoeko, D.R. Halpern, and P.P. Niiler, 1981: Variability in the upper ocean during MILE. Part I: The heat and momentum balances. *Deep-Sea Res.*, **28**, 1427-1451.
- Gould, W.J., 1985: Physical oceanography of the Azores Front, *Prog. Oceanogr.*, **14**, 167-190.
- Käse, R.H., J.F. Price, P. Richardson, and W. Zenk, A quasi-synoptic survey of the thermocline circulation and water masses distribution within the Canary Basin. *J. Geophys. Res.* **91**, 9739-9748, 1986.
- Kirwan, A.D. Jr, G. McNally, and J. Coehlo, 1976: Gulf stream Kinematics inferred from a satellite tracked drifter. *Journal of Physical Oceanography*, **6**, 750-755.
- Kirwan, A.D., Jr., G.J. McNally, E. Reyna, and W.J. Merrell, Jr., 1978: The near-surface circulation of the eastern north Pacific. *J. Phys. Oceanogr.*, **8**, 937-945.
- Kraus, E.B., and J.S. Turner, 1967: A one-dimensional model of the seasonal thermocline: II, The general theory and its consequences. *Tellus*, **19**, 98-106.
- Krauss, W., and C.W. Böning, 1987: Lagrangian properties of eddy fields in the northern north Atlantic as deduced from satellite-tracked buoys. *J. Marine Res.*, **45**, 259-291.
- McNally, G.J., 1981: Satellite-tracked buoy observations of the near-surface flow in the eastern mid-latitude north Pacific. *J. Geophys. Res.*, **86**, 8022-8030.

- McNally, G.J., D.S. Luther, and W.B. White, 1989: Subinertial frequency response of wind-driven currents in the mixed layer measured by drifting buoys in the midlatitude north Pacific. *J. Phys. Oceanogr.*, **19**, 290-300.
- Niiler, P.P., R.E. Davis, and H.J. White, 1987: Water-following characteristics of a mixed layer drifter. *Deep-Sea Res.*, **34**, 1867-1881.
- Niiler, P.P., and E.B. Kraus, 1977: One-dimensional models of the upper ocean. *Modeling and Prediction of the Upper Layers of the Ocean*, E.B. Kraus, Ed., Pergamon, 143-172.
- Niiler, P.P., and J.D. Paduan, 1993: Wind-driven motions in the northeast Pacific as measured by Lagrangian drifters. *J. Phys. Oceanogr.* Submitted.
- Niiler, P.P., A.S. Sybrandy, K. Bi, P-M. Poulain, and D. Bitterman, 1993: Measurements of the water-following capability of Holey-sock and TRISTAR drifters. *J. Atm. & Ocean Tech.*, Submitted.
- Paduan, J.D., and R.A. deSzoek, 1986: Heat and energy balances in the upper ocean at 50°N, 140°W during November 1980 (STREX). *J. Phys. Oceanogr.*, **16**, 25-38.
- Paduan, J.D., R.A. deSzoek, and J.G. Richman, 1988: Balances of heat and momentum at 33.5°N, 127°W in the upper ocean during the Mixed-Layer Dynamics Experiment. *J. Geophys. Res.*, **93**, 8147-8160.
- Paduan, J.D., and P.P. Niiler, 1990: A Lagrangian description of motion in northern California Coastal Transition Filaments. *J. Geophys. Res.*, **95**, 18095-18110.
- Paduan, J.D., and P.P. Niiler, 1993: Structure of velocity and temperature in the northeast Pacific as measured with Lagrangian drifters in fall 1987. *J. Phys. Oceanogr.*, **23**, 585-600.
- Pollard, R.T., R.B. Rhines, and R.O.R.Y. Thompson, 1973: The deepening of the wind mixed layer. *Geophys. Fluid Dyn.*, **3**, 381-404.
- Poulain, P.M., and P.P. Niiler, 1989: Statistical analysis of the surface circulation in the California Current System using satellite-tracked drifters. *J. Phys. Oceanogr.*, **19**, 1588-1603.

- Price, J.F., R.A. Weller, and R. Pinkel, 1986: Diurnal cycling: Observations and models of the upper ocean response to diurnal heating, cooling, and wind mixing. *J. Geophys. Res.*, **91**, 8411-8427.
- Richardson, P.H., and C.M. Wooding, 1985: Surface drifter measurements in the Atlantic North Equatorial Countercurrent 1983-1985. Woods Hole Oceanographic Institution 85-31, 117 pp.
- Richardson, P.H., 1983: Eddy Kinetic energy in the North Atlantic from surfers drifters. *J. Geophys. Res.*, **88**, 4355-4367.
- Stramma, L. and T.J. Müller, 1989: Some observations of the Azores Current and the North Equatorial Current. *J. Geophys. Research*, **94**, 3181-3186.
- Sybrandy, A.L., and P.P. Niiler, 1991: WOCE/TOGA Lagrangian Drifter Construction Manual, SIO Reference 91/6, Scripps Institution of Oceanography, University of California, San Diego, WOCE Report Number 63.
- Tabata, S., 1965: Variability of oceanographic conditions at Ocean Station "P" in the Northeast Pacific Ocean. *Trans. Roy Soc. Can., Ser 4*, **3**, 367-418.
- Taylor, G.I., 1921: Diffusion by continuous movements. *Proc. London Math. Soc.*, **20**, 196-212.
- Weller, R.A., and R.E. Davis, 1980: A vector measuring current meter. *Deep-Sea Res.*, **27**, 565-582.

## INITIAL DISTRIBUTION LIST

		No. Copies
1.	Defense Technical Information Center Cameron Station Alexandria, VA 22304-6145	2
2.	Library, Code 52 Naval Postgraduate School 411 Dyer Rd, Rm 104 Monterey, CA 93943-5101	2
3.	Superintendent Attn: Chairman, Department of Oceanography Code OC/Co Naval Postgraduate School Monterey, CA 93943-5000	1
4.	Superintendent Attn: Assistant Professor J. D. Paduan Code OC/Pd Naval Postgraduate School Monterey, CA 93943-5000	1
5.	Library Scripps Institution of Oceanography P.O. Box 2367 La Jolla, CA 92037	1
6.	Professor Pearn P. Niiler Box 0230, Scripps Institution of Oceanography University of California, San Diego La Jolla, CA 92093-0230	1
7.	Dr. Jean Rolland Centre de Meteorologie Marine BP70 29263 Plouzane Cedex FRANCE	1
8.	Dr. Pierre Poulain SACLANT Undersea Research Center APO New York 09019-5000	1

(continued)



- |     |  |   |
|-----|--|---|
| 9.  | Dr. Steve Ramp<br>Office of Naval Research<br>Code 332PO<br>800 N. Quincy Street<br>Arlington, VA 22217-5660             | 1 |
| 10. | Ms. Mayra Pazos<br>NOAA/AOML<br>4301 Rickenbacker Causeway<br>Miami, FL 33149  | 1 |
| 11. | MARISTAT<br>U.A.G.<br>00100 ROMA<br>ITALY  | 1 |
| 12. | MARISTAT<br>4° REP S.A.M.<br>00100 ROMA<br>ITALY   | 1 |
| 13. | Italian Embassy<br>Office of the Naval Attaché<br>5301 Wisconsin Av, NW<br>Washington, D.C. 20015                        | 1 |
| 14. | Director<br>ISTITUTO IDROGRAFICO DELLA MARINA<br>PASSO OSSERVATORIO 4<br>16100 GENOVA<br>ITALY                           | 1 |
| 15. | Meteorology Department<br>Code Mr/Hy<br>Naval Postgraduate School<br>589 Dyer Rd., Rm 252<br>Monterey, CA 93943-5114     | 1 |
| 16. | Director Naval Oceanography Division<br>Naval Observatory<br>34th and Massachusetts Avenue, NW<br>Washington, D.C. 20390 | 1 |
| 17. | Commander<br>Naval Oceanography Command<br>Stennis Space Center<br>MS 39539-5000   | 1 |

(continued)

- |  |   |
|--|---|
| 18. Commanding Officer<br>FLENUMOCEANCEN<br>7 Grace Hopper Ave., Stop 4<br>Monterey, CA 93943-0001-0120                  | 1 |
| 19. Technical Director<br>Naval Research Laboratory<br>Stennis Space Center, MS 39529-5004                               | 1 |
| 20. Technical Director<br>Naval Research Laboratory<br>7 Grace Hopper Ave., Stop 2<br>Monterey, CA 93943-5502            | 1 |
| 21. Chief of Naval Research<br>800 N. Quincy Street<br>Arlington, VA 22217   | 1 |
| 22. Library<br>Department of Oceanography<br>University of Washington<br>Seattle, WA 98105                               | 1 |
| 23. Library<br>CICESE<br>P.O. Box 4803<br>San Ysidro, CA 92073   | 1 |
| 24. Library<br>College of Oceanography<br>Oceanography Admin Bldg. 104<br>Oregon State University<br>Corvallis, OR 97331 | 1 |
| 25. Commander<br>International Ice Patrol<br>Avery Point<br>Groton, CT 06340   | 1 |
| 26. NOAA Library<br>7600 Sand Point Way, NE<br>Building 3<br>Seattle, WA 98115   | 1 |